Interannual Variability of Temperature, Water Vapor, and Clouds in the Tropical Tropopause Layer

Aodhan John Sweeney[1] and Qiang Fu[2]

[1]University of Washington
[2]Department of Atmospheric Sciences ,University of Washington

November 4, 2023

Interannual Variability of Zonal Mean Temperature, Water Vapor, and Clouds in the Tropical Tropopause Layer

Aodhan Sweeney[1] and Qiang Fu[1]

[1]University of Washington, Department of Atmospheric Sciences.
Corresponding author: Aodhan Sweeney (aodhan@uw.edu)

Key Points:

- The interannual variability in the cold point tropopause temperature averaged over 15°S-15°N is driven by stratospheric processes
- This cold point tropopause temperature residual after regressing out large-scale modes is still correlated with stratospheric temperature
- The portion of the shallow branch BDC, which is independent of the eddy heat flux BDC index, is an important source of TTL variability

Abstract

Water vapor and cirrus clouds in the tropical tropopause layer (TTL) are important for the climate and are largely controlled by temperature in the TTL. On interannual timescales, both stratospheric and tropospheric modes of the large-scale variability could affect temperatures in the TTL. Here multiple linear regression (MLR) is used to investigate explained variance in the cold point tropopause temperature (CPT), cold point tropopause height (CPZ), 83 hPa water vapor (WV83), 83 hPa ozone ($O_3$83), and total cirrus cloud fraction with cloud base (TTLCCF) and top (ALLCF) above 14.5 km, all averaged over 15°N - 15°S. Predictors of the MLR are a set of stratospheric and tropospheric large-scale modes of variability. The MLR explains significant variance in CPT (76%), CPZ (78%), WV83 (65%), $O_3$83 (62%), TTLCCF (52%), and ALLCF (36%). The interannual variability of CPT and WV83 is dominated by stratospheric processes associated with the Quasi-Biennial Oscillation (QBO) and Brewer-Dobson Circulation (BDC), whereas the variability of CPZ, $O_3$83, TTLCCF and ALLCF is also controlled by 500 hPa temperature (T500). Residual variability in CPT and CPZ not captured by the MLR are further significantly correlated to stratospheric temperature. It is shown that the portion of the BDC's shallow branch missed by the eddy heat flux based BDC index contributes significant amounts of the explained variances.

Plain Language Summary

Between the tropical upper troposphere and lower stratosphere, water can exist as either vapor or ice. The amount of water that enters the stratosphere depends on the portion of vapor that is frozen out by the coldest temperature that air experiences in this region, which on interannual timescales could be modulated by both large-scale stratospheric and tropospheric modes of variability. Here we show that 76%, 65%, and 52% of the interannual variance in cold point temperature, water vapor at 83 hPa, and ice cloud fraction in this region can be explained using a multiple linear regression (MLR), where the predictors are the modes of the large-scale variability. Stratospheric processes are much more important in controlling the interannual variance of cold point temperature and water vapor at 83 hPa, but notably, the height of the cold

point is controlled by both stratospheric and tropospheric processes. Residual variability of the cold point temperature not captured by the MLR is still connected to temperature variability in the stratosphere.

1 Introduction

The tropical tropopause layer (TTL) is a transition layer between the tropical troposphere and stratosphere and extends from the level of zero net radiative heating to the maximum height where clouds still exist (~14.5 to ~18.5 km) (e.g., Gettelman et al., 2004; Fu et al., 2007; Fueglistaler et al., 2009). A crucial component of the TTL is the water vapor and ice that exists there. Water vapor in the TTL can transit into the stratosphere, where it has significant impacts on Earth's radiation budget and stratospheric ozone (Mote et al., 1996; Forster and Shine, 1999; Kirk-Davidoff et al., 1999; Fueglistaler and Haynes, 2005; Solomon et al., 2010; Joshi et al., 2010; Flury et al., 2012; Ding & Fu, 2018; Randel and Park, 2019). Ice in this region exists as thin and extensive cirrus referred to as TTL cirrus clouds. These clouds can impact the TTL's local radiative heating rate, which may influence the upwelling and temperatures in the TTL (McFarquhar et al., 2000; Corti et al., 2006; Yang et al., 2010; Dinh et al., 2010; Fu et al., 2018; Wang and Fu, 2021). These cirrus clouds might also contribute a warming effect on the surface (Zhou et al., 2014). Despite their importance, climate models have difficulty simulating stratospheric water vapor concentrations and TTL cirrus clouds (Gettelman et al., 2009; Gettelman et al., 2010; Randel and Jensen, 2013; Hardiman et al., 2015; Wang and Fu, 2021).

The water vapor going into the stratosphere is largely regulated by the coldest temperatures that air experiences in the TTL, especially during boreal winter (Holton and Gettelman, 2001). Cold temperature anomalies in the TTL can largely limit the entry of water vapor into the stratosphere through the formation of TTL cirrus clouds-(Jensen, 1996; Flury et al., 2012; Jensen et al., 2013; Randel and Jensen, 2013). Temperature variability in this region is a result of both stratospheric and tropospheric modes of large-scale variability (Randel and Wu, 2015; Charlesworth et al., 2019; Lu et al., 2020). Observed interannual variations in TTL temperature, water vapor, and clouds have been linked to stratospheric modes including the Quasi-Biennial Oscillation (QBO) and Brewer Dobson circulation (BDC) and tropospheric modes including the El Nino Southern Oscillation (ENSO) and Madden-Julian Oscillation (MJO) (Virts and Wallace, 2010; Eguchi and Kodera, 2010; Liang et al., 2011; Davis et al., 2013; Li and Thompson, 2013; Virts and Wallace, 2014; Ding and Fu, 2018; Tseng and Fu, 2017a; Tseng and Fu, 2017b; Ye et al., 2018; Sweeney et al., 2023). Wave activity on a variety of temporal and spatial scales can also impact TTL temperatures and cirrus clouds based on both observational and modeling studies (Boehm and Verlinde, 2000; Grise and Thompson, 2013; Kim and Alexander, 2015; Podglajen et al., 2016; Kim et al., 2016; Podglajen et al., 2018; Chang and L'Ecuyer, 2020; Bramberger et al., 2022).

An open question remains to what extent these observed interannual variations are governed by stratospheric versus tropospheric processes (Garfinkel et al., 2013; Fu, 2013; Ding and Fu, 2018). This question is important because the decadal TTL variability has been linked to both (Solomon et al., 2010; Garfinkel et al., 2013; Xie et al., 2014; Lu et al., 2020). Despite the different sources of the variability, their influence on the TTL variability may involve common mechanisms by e.g., modulation of the TTL upwelling, complicating the partitioning of the sources (Austin and Reicher, 2008; Lin et al., 2017). This question is also important because connections between TTL variables and the modes of large-scale variability found in observations may help validate models' representation of the TTL. This study attempts to shed light on this question by examining key target variables in the TTL like temperature, water vapor, ozone, and cloud fraction observed from radio occultations, the Microwave Limb Sounder aboard the Aura satellite, and the CALIOP instrument. The explained variance of these target variables is investigated by employing a multiple linear regression (MLR) where predictors are the QBO, BDC, T500, and MJO (Dessler et al., 2013; Dessler et al., 2014; Tseng and Fu, 2017a; Wang et al., 2019).

2 Data

2.1 Target Variables

2.1.1 Temperature

Temperature data come from Radio Occultation (RO) profiles from the COSMIC-1 and 2 as well as the MetOp-A, B, and C satellites, archived at the University Corporation for Atmospheric Research (Anthes et al., 2008; Schreiner et al., 2020). Data was preprocessed using the level 2 WetPrf product from June 2006 to December of 2021 (Sweeney and Fu, 2021). These RO temperature profiles have high accuracy (less than 0.1 K). RO data have high vertical resolution (~0.5 km) in the TTL, but coarser horizontal resolution of about 200 km (Kursinski et al., 1997; Kuo et al., 2004; Zeng et al., 2019). The vertical temperature gradient and cold point tropopause temperature and height are also calculated from the RO temperature data.

2.1.2 Clouds

Cloud fraction data comes from the Cloud-Aerosol Lidar with Orthogonal Polarization (CALIOP) instrument aboard the CALIPSO satellite (Winker et al, 2010). CALIOP can provide information of cloud layers with optical depth as small as 0.01 or less, ideal for TTL cirrus cloud identification. We use the Level 2 V4.2 5-km Merged Layer Products from June of 2006 to December of 2021, using only nighttime measurements to avoid solar contamination of the lidar signals (Thorsen et al., 2013; Thornberry et al., 2017). Cloud fraction is derived from the lidar data as the number of detections of a cloud divided by the total number of observations in each 2.5°x2.5° grid cell at a given level. Positive cloud identifications require Cloud-Aerosol Distinction (CAD) values of greater than 30. This study uses an adapted version of the Level 2 V4.2 data for clouds above the lapse rate tropopause (Tseng and Fu, 2017b; Sweeney et al., 2023).

Two different categories of clouds are identified in this study: TTL cirrus clouds which are defined as clouds with bases above 14.5 km, and All clouds which are defined as clouds with tops above 14.5 km irrespective of their cloud base. The 14.5 km altitude is approximately the level of zero net radiative heating in the tropical atmosphere (Gettelman et al., 2004; Fu et al., 2007; Tseng and Fu, 2017a). We consider TTL cirrus and All clouds separately because TTL cirrus clouds are more relevant for the dehydration of the TTL, while All clouds are more relevant for the total energy budget of the tropics (Corti et al., 2006; Jensen et al., 2013; Sokol and Hartmann, 2020; Sweeney et al., 2023).

Both the TTL cirrus cloud fraction and All cloud fraction are turned into one-dimensional monthly timeseries referred to as TTLCCF and ALLCF respectively. TTLCCF measures total cloud fraction similarly to TTL cirrus cloud fraction described above but does not consider the vertical extent of the TTL cirrus cloud (i.e., only measures whether a TTL cirrus cloud is present, and not its vertical profile). ALLCF only measures whether a cloud top above 14.5 km is present, and not the vertical profile of the cloud.

2.1.3 Water Vapor and Ozone

Water vapor data come from the Microwave Limb Sounder (MLS) onboard the Aura Satellite (Read et al., 2007). Results regarding ozone concentrations also come from this MLS. MLS measurements began in August 2004 and continue until present day. Water vapor and ozone mixing ratios come from monthly mean Level 3 version 5 MLS data from June 2006 to December of 2021 (Livesey et al., 2021). Tropical lower stratospheric water vapor is primarily sourced from the troposphere, and transits slowly upward from the tropopause (Randel and Park., 2019). Because we are particularly interested in the interannual variability of lower-stratospheric water vapor, all water vapor data is lagged by one month to account for the slow transit time into the lower stratosphere.

2.2 Predictors

2.2.1 Quasi-Biennial Oscillation (QBO) index

The QBO is the main mode of the large-scale variability in the tropical stratosphere (Baldwin et al., 2001) and is a stratospheric process. The QBO index is defined using the monthly mean 50 hPa zonal wind averaged over 10°S-10°N from ERA5 (Hersbach et al., 2020). We let the QBO index lead the TTL variables by two months to account for the QBO temperature anomaly's descent to the cold point tropopause (Dessler et al., 2013; Dessler et al., 2014; Ding and Fu, 2018; Tseng and Fu, 2017a; Ye et al., 2018; Tian et al., 2019).

2.2.2 Madden Julian Oscillation (MJO) index

The MJO is the dominant mode of intraseasonal variability in the tropical atmosphere and is a tropospheric process (Madden and Julian, 1971). The MJO index used here is the second principal component of the velocity potential index (Ventrice et al., 2013). Maximums in this MJO index are associated with peak MJO-related convection over the western Pacific and suppressed convection over the eastern Indian Ocean (Virts and Wallace, 2014; Tseng and Fu, 2017a). We use the velocity potential index provided by the NOAA Physical Science Laboratory (https://www.psl.noaa.gov/mjo/mjoindex/).

2.2.3 Temperature at 500 hPa (T500)

The 15°S-15°N 500 hPa temperature (T500) from the ERA5 reanalysis measures tropospheric temperature. ENSO is the dominate mode of tropospheric temperature variability (Philander et al., 1990). T500 is highly correlated with a three-month lead of the ENSO MEIv2 index (r=0.73) and thus implicitly captures much of the ENSO variability (Dessler et al., 2013; Wang et al., 2019; Marsh and Garcia, 2007). T500 can impact the TTL through longwave heating, changing tropical convective activity, and other processes (Lin et al., 2017; Ye et al., 2018). Increases in T500 can dynamically induce upwelling in the TTL through the eddy momentum flux convergence in the tropical upper troposphere driven by convective latent heat (Boehm and Lee, 2003; Deckert and Dameris, 2008; Garny et al., 2011), which has been considered part of the BDC in some studies (e.g., Boehm and Lee, 2003) but not in others (e.g., Wu and Zheng, 2022). T500 thus impacts the TTL through both thermodynamic and dynamic processes and is considered a tropospheric process here.

2.2.4 Eddy Heat Flux Based Brewer-Dobson Circulation index (BDC_{EHF})

The BDC influences TTL variability by modulating the TTL upwelling (Haynes et al., 1991; Yulaeva et al., 1994; Holton et al., 1995). The deep branch of the BDC is driven by extratropical stratospheric waves, which is linked to the meridional eddy heat flux in the lower stratosphere (Li and Thompson, 2013). To quantify the BDC deep branch, we calculate the monthly averaged zonal mean meridional eddy heat flux at 100 hPa averaged over 25°-90° in the northern hemisphere minus that of the southern hemisphere (Tseng and Fu, 2017a; Randel et al., 2002). We refer to this BDC index based on the eddy heat flux as BDC_{EHF}. Temperatures are correlated with wave driving during the current and previous months; thus, the BDC_{EHF} index is created using a three-month running mean centering on the previous month (Lin et al., 2009; Li and Thompson, 2013; Fu et al., 2015; Tseng and Fu, 2017a). This BDC_{EHF} index is calculated using 6 hourly ERA5 data from 2006-2021. Note that in addition to the BDC deep branch, the eddy heat flux-based index BDC_{EHF} may also include a portion of the shallow branch of the BDC (Grise and Thompson, 2013).

<u>2.2.5 Partial Shallow Branch of the Brewer-Dobson Circulation index (BDC_{PSB})</u>

In addition to extratropical stratospheric waves, tropical and subtropical waves also drive the TTL upwelling. The upwelling due to the subtropical waves is associated with the shallow branch of the BDC (Grise and Thompson, 2013; Abalos et al., 2014; Ortland and Alexander, 2015). The shallow branch of the BDC thus also influences TTL variability by modulating the TTL upwelling. Note that in this study, the upwelling driven by equatorial planetary waves (Boehm and Lee, 2003; Deckert and Dameris, 2008; Garny et al., 2011), which is related to T500, is not considered as part of the BDC. We attempt to quantify the role of the shallow branch that may be missed by the BDC_{EHF} by using the residual TTL upwelling after removing the impacts of the QBO, T500, and BDC_{EHF}. This residual TTL upwelling which represents the partial shallow branch of the BDC is referred to as BDC_{PSB}.

To quantify the TTL upwelling, we calculate the upwelling at 100 hPa over 15°S-15°N using the transformed Eulerian mean (TEM) vertical velocity, for 2006-2021 using the 6-hourly ERA5 reanalysis following equation (1) (e.g., Haynes et al., 1991; Rosenlof et al., 1995; Randel et al., 2008; Abalos et al., 2012).

$$\overline{w*} = \overline{w} + \frac{1}{a\cos\emptyset}\frac{\partial}{\partial\emptyset}\left(\cos\emptyset\frac{\overline{v'T'}}{S}\right) \quad (1)$$

where $\overline{w*}$ is the zonal mean TEM residual vertical velocity, $\overline{w}$ is the zonal mean vertical velocity from ERA5, a is the radius of the earth, v is the meridional velocity, T is the temperature, and S is the stability parameter $S=\frac{HN^2}{R}$, a function of the Brunt-Vaisala frequency (N), with H = 7 km and R = 287 $m^2s^{-2}K^{-1}$. Overbars and primes represent zonal means and zonal deviation respectively. After computing the upwelling, we regress out the combined impact of the QBO, T500, and BDC_{EHF} using a MLR (Garfinkel and Hartmann, 2008; Abalos et al., 2014). The 100 hPa upwelling before regressing out QBO, T500 and BDC_{EHF} has a correlation coefficient of -0.32, 0.49, and 0.46, respectively, with the QBO, T500 and BDC_{EHF} (the MLR using the QBO, BDC_{EHF}, and T500 can explain 60% of the variability in the raw 100 hPa upwelling).

Because this study focuses on interannual variability, all data is deseasonalized and detrended. The target variables and predictors are created as the monthly anomalies by removing the monthly climatology from June 2006 – December 2021. Before removing linear trends in each timeseries, trends are computed using linear regression and are provided in Table S1. No trend is significant at the 95% confidence level besides that of the ALLCF timeseries, but this trend is not further investigated here.

3 Results

The climatology and interannual standard deviation of tropical upper-tropospheric and lower-stratospheric temperature, water vapor, vertical temperature gradient, and cloud fractions from June 2006 to December 2021 are provided in Figure S1. Importantly, the interannual variability for all these variables maximizes within 15°S-15°N. A significant cloud fraction variance occurs above the climatological cold point tropopause (Figs. S1I and S1J). Cloud fraction variability above the climatological cold point tropopause may be related to coincident changes in tropopause height. Figures S1 K-L show the interannual variance in a vertical coordinate relative to the cold point tropopause height, showing cloud fraction variability to maximize below the cold point tropopause.

3.1 Target Variable Correlations with Modes of Large-Scale Variability

Figure 1 shows the correlation between target variables with the zonal mean cold point tropopause temperature (CPT) averaged over 15°S-15°N (row 1), and the correlations of target variables with the modes of large-scale variability (row 2-6). Although the CPT is not a mode of variability, it is critically important for stratospheric water vapor (e.g., Randel and Jensen, 2013) and is highly correlated with TTL cirrus cloud fraction (Tseng and Fu, 2017a). CPT is significantly correlated with stratospheric temperatures but has little correlation with those in the troposphere (Fig. 1A), suggesting that processes controlling the CPT also impact the tropical lower stratosphere (Randel and Wu, 2015). Lower-stratospheric water vapor reaches correlations of ~0.8 at the cold point tropopause (Fig. 1B), indicative of the temperature control of lower-stratospheric water vapor. Water vapor is transported vertically into the stratosphere over the tropics by the BDC (Brewer et al., 1949; Mote et al., 1996; Flury et al., 2012; Flury et al., 2013), and is also transported between lower and higher latitudes through quasi-horizontal isentropic mixing (Randel and Park, 2019). These processes are responsible for the convex shape of peak correlations between CPT and water vapor in the TTL (Fig. 1B). CPT is strongly anticorrelated with equatorial TTL cirrus and All cloud fraction (Figs. 1D-E). Positive correlations between CPT and cloud fraction exist near the subtropical lapse rate tropopause, the inverse of the correlation between CPT and subtropical temperature. The strong correlations between CPT and the target variables stress the temperature control of the water partitioning between vapor and clouds in the TTL. Correlations between the CPT and target variables extends to higher latitudes in Figure S2.

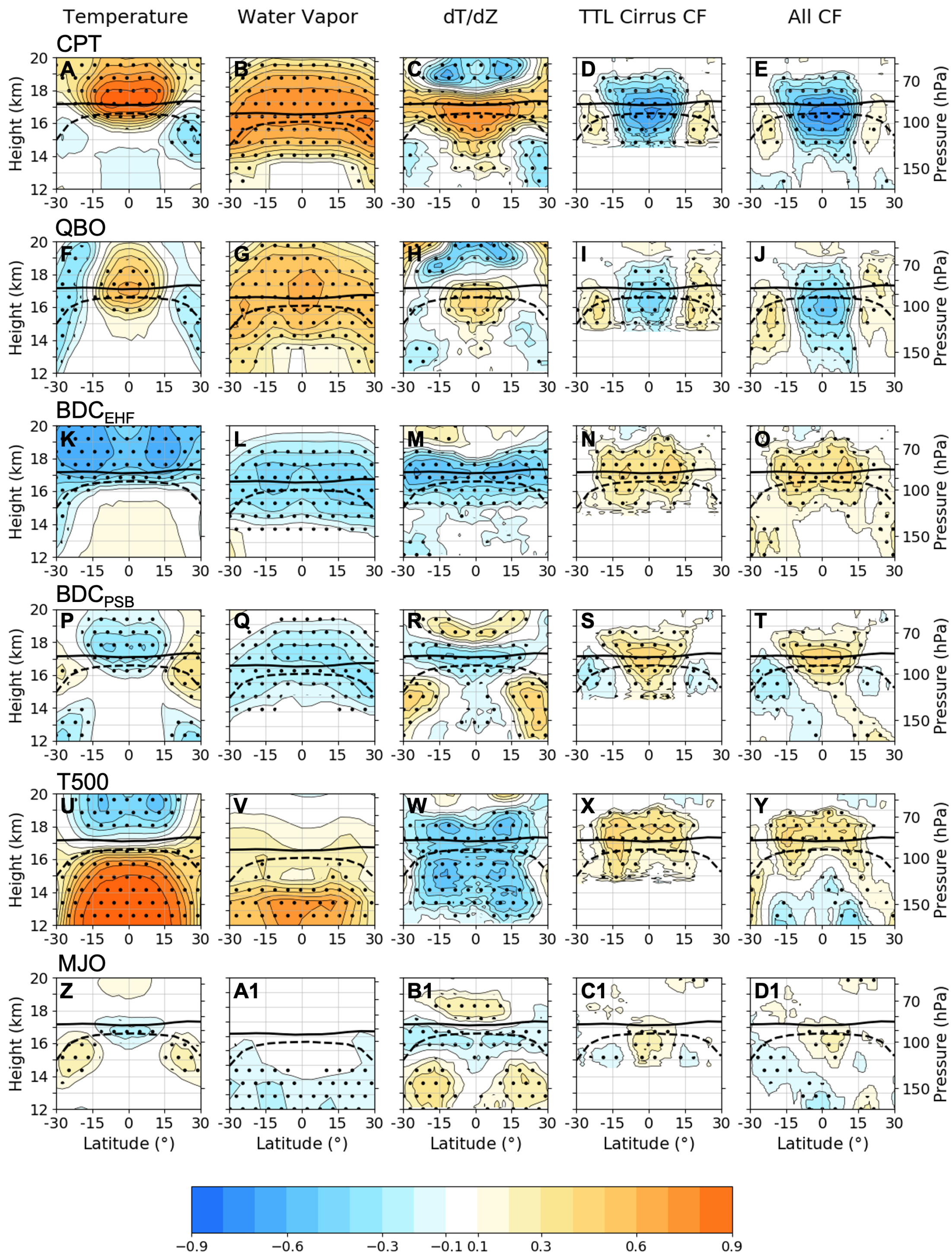

Figure 1: Correlations in tropical upper troposphere and lower stratosphere between target variable monthly anomalies and modes of the large-scale variability, except for row 1 that shows correlation between target variables and cold point temperature (CPT) averaged over 15°S-15°N. Stippling indicates significance at 95% confidence and the solid (dashed) black line is the climatological mean cold point (lapse rate) tropopause.

The QBO and temperature are correlated in the equatorial TTL, but anticorrelated in the subtropical TTL due to the QBO's meridional circulation (Fig. 1F) (Plumb and Bell, 1982; Baldwin et al., 2001; Pahlavan et al., 2021). QBO correlations with cloud fraction are inverse to those of temperature (Fig. 1I-J). Subtropical cloud fraction correlations are weaker than the equatorial signal, possibly due to the weaker QBO-temperature correlations and the lower relative humidity. Significant QBO correlations with All cloud fraction reach into the troposphere as low as ~13 km (Fig. 1J), below the region of peak QBO power (Sweeney et al., 2023). This deep QBO signature may be due to convective feedbacks (Tegtmeier et al., 2020). The QBO and water vapor correlations peak at the equatorial tropopause and are spread latitudinally due to quasi-isentropic mixing (Fig. 1G). The QBO impacts lapse-rate tropopause temperature out to near 50° in both hemispheres with weak statistically significant implications for cloud fraction (Fig. S2).

Increases in BDC_{EHF} cause upwelling and cooling in the tropical lower stratosphere (Fig. 1K) (Mote et al., 1996; Plumb and Eluszkiewicz, 1999; Randel et al., 2002). Decreasing temperature and vertical temperature gradient promotes cloud formation at and above the climatological mean tropopause (Figs. 1N-O). Notably, temperature and CPT correlations can be largely inferred from temperature and QBO minus temperature and BDC_{EHF}, both in the TTL (i.e., Fig. 1A resembles Fig. 1F minus Fig. 1K), and globally (Fig. S2).

The BDC_{PSB} index is related to the TTL cold anomalies flanked by subtropical upper-tropospheric warm anomalies (Fig. 1P), with tropospheric cold anomalies underneath the warm anomalies. BDC_{PSB} is also anticorrelated with lower-stratospheric water vapor (Fig. 1Q). BDC_{PSB} cloud fraction correlations peak near the equatorial tropopause (Figs. 1S-T). The BDC_{PSB} and temperature correlation pattern resembles the temperature tendencies caused by subtropical upper-tropospheric waves which can cause subseasonal variability in the shallow branch of the BDC (Grise and Thompson, 2013; Abalos et al., 2014). The shallow branch of the BDC is also driven by subtropical stratospheric waves, which is considered in BDC_{EHF} (Grise and Thompson, 2013). Figures 1P-T show that BDC_{PSB} is well correlated with the target variables and is an important component of TTL variability.

T500 measures tropospheric temperature and is positively correlated with temperatures below the tropopause (Fig. 1U). Increased T500 dynamically induces upwelling and cooling of the lower stratosphere (Randel et al., 2009; Calvo et al., 2010; Shepard and McLandress, 2011; Lin et al., 2017). The net result of warming below the tropopause and cooling above is a reduction of vertical temperature gradient throughout the TTL (Fig. 1W). T500 has significant correlations with cloud fraction near and above the climatological tropopause (Davis et al., 2013; Avery et al., 2017; Ye et al., 2018). The correlation between T500 and lower-stratospheric water vapor is insignificant (Fig. 1V), consistent with T500's weak impact on CPT ($r=-0.11$) (Liang et al., 2011; Konopka et al., 2016; Diallo et al., 2018; Garfinkel et al., 2021; Ziskin Ziv et al., 2022). This may be expected given that much of the T500 variability is related to ENSO which shows a strong longitudinal dipole impact on CPT which cancels in the zonal mean (Randel et al., 2000; Scherllin-Pirscher et al., 2012; Tseng and Fu, 2017a; Garfinkel et al., 2021). Interpreting the physical mechanism by which T500 influences the CPT is complicated due to competing processes, but it is important to understand the response of stratospheric water vapor to global warming. Discussion of the relevant mechanisms by which T500 may impact the TTL is provided in Section 3.3. The correlation between T500 and global temperature (Fig. S2) reveals a meridional circulation in the tropical and subtropical lower stratosphere.

The last row in Fig. 1 shows correlations between the MJO and target variables. The MJO is the main mode of intraseasonal variability in the tropics (Madden and Julian, 1971), and impacts subseasonal variability of temperature and cloud fraction in the TTL (Virts and Wallace., 2014; Virts et al., 2010). MJO-temperature correlations have a distinct pattern of weak equatorial (subtropical) anticorrelation (correlation) (Grise and Thompson, 2013). Results of Fig. 1 show that the MJO only weakly correlates with the TTL target variables. This is partly because the monthly averaging of the MJO index and target variables smooths the intraseasonal variability.

3.2 Explained Variances in Target Variables from MLR

We next use the modes of the large-scale variability as predictors in a multiple linear regression (MLR) to quantify the explained variance of cold point tropopause temperature (CPT), water vapor at 83 hPa (WV83), cold point tropopause height (CPZ), ozone concentrations at 83 hPa ($O_3$83), total TTL cirrus cloud fraction (TTLCCF), and All cloud fraction (ALLCF), all averaged over 15°S-15°N.

Explained variance is quantified using the adjusted R^2, which accounts for artificial inflation due to collinearity in the MLR and is always smaller than the true R^2. The unique contribution of explained variance to the adjusted R^2 from each predictor is not possible unless predictors are independent of each other. A correlation matrix among all predictors and target variables is provided in Figure S3. The predictors show small correlations with each other over the period investigated, which are all statistically insignificant. For example, the correlation is -0.07 between QBO and BDC_{EHF}, and 0.14 between T500 and BDC_{EHF}. To account for these non-zero correlations, we partition the adjusted R^2 into the unique contributions from the QBO, BDC_{EHF}, BDC_{PSB}, T500, and MJO by recursively adding each predictor to our MLR model while also permuting the order of addition. This allows for an estimate of unique explained variance (Lindeman et al., 1980). We note that this method is not perfect because the predictors are not entirely independent but provides an estimate of the unique explained variance from each mode of variability.

Figure 2 shows the MLR's explained variance of CPT (76%), WV83 (65%), TTLCCF (52%), ALLCF (36%), CPZ (78%), and $O_3$83 (62%). Stratospheric processes (i.e., the QBO, BDC_{EHF}, and BDC_{PSB}) dominate the variance captured in CPT, WV83, and ALLCF. T500 contributes more to TTLCCF and $O_3$83, and to nearly half of the explained variance in CPZ. The MJO minimally affects any target variable. BDC_{PSB} explains substantial variances in CPT, WV83, and TTLCCF, and should be considered an important component of the TTL variability. The MLR here significantly enhances explained variance of CPT and TTLCCF compared to previous studies (Tseng and Fu, 2017a) by considering BDC_{PSB}.

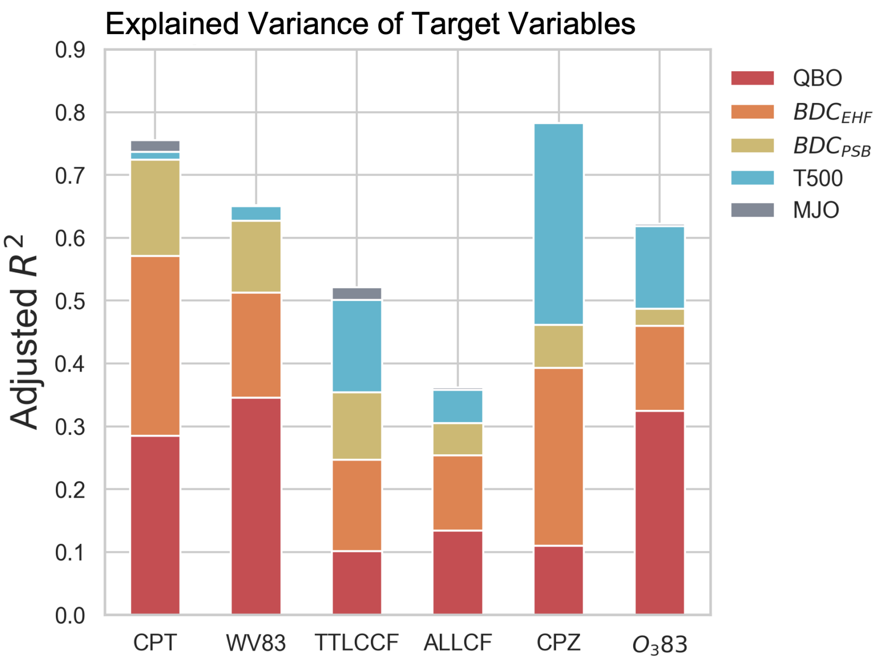

Figure 2: Adjusted R^2 from multiple linear regression model applied to target variables using modes of the large-scale variability as predictors. Colored sections indicate the estimated contribution to the adjusted R^2 from each predictor.

Tseng and Fu (2017a) stressed the importance of CPT for TTLCCF variability. A linear regression using only CPT as a predictor explains 41% of TTLCCF variance, while the MLR in Fig. 2 explains 52%. Including CPT as an additional predictor in the MLR for TTLCCF only increases the explained variance slightly from 52 to 54%, indicating that most of the CPT control of TTLCCF has already been included in our MLR. But this is not true for WV83 whose explained variance increases by 8% (from 65% to 73%) when including CPT as an additional predictor. Thus, a better understanding of the CPT variance would help explain WV83 variance. The cloud fraction explained variance is strongly dependent on altitude, where at 17 km the MLR explains over 60% of the variance in TTL cirrus and All cloud fraction, possibly due to the higher frequency of laminar tropopause cirrus at these altitudes (Wang et al., 2019).

TTL ozone variability is primarily due to the TTL upwelling and in-mixing of ozone depleted tropospheric air (Randel et al., 2007; Konopka et al., 2009; Solomon et al., 2016; Wang and Fu, 2021; Wang and Fu, 2023). Long-term ozone concentrations at a fixed height in the TTL may decrease due to the strengthening of the tropical upwelling associated with the BDC, and/or tropospheric expansion due to warming (Banerjee et al., 2016; Chiodo et al., 2018; Wang et al., 2020; Match and Gerber, 2022). Fig. 2 shows that the MLR explains 62% of $O_3$83 variance, with about half attributed to the QBO while the rest is split roughly equally between BDC_{EHF} and T500. Despite the QBO's important role in determining $O_3$83, decadal changes in $O_3$83 due to the QBO are uncertain due to ambiguity in the QBO response to global warming (e.g., Richter et al., 2020; Fu et al. 2020). Our results suggest that both T500 and the BDC_{EHF} affect $O_3$83 (Match and Gerber, 2022). However, the T500 influence on $O_3$83 may operate via a dynamic response in the TTL upwelling. Further discussion on T500's impact on target variables including $O_3$83, can be found in Section 3.3.

A key result of Fig. 2 is that despite the strong correlation between CPT and CPZ (r=-0.74) the interannual variability of CPT is predominately explained by stratospheric processes, while CPZ's variability is equally explained by stratospheric and tropospheric processes. In Figure 3, we further examine how CPT covaries with the tropospheric and stratospheric temperatures. Fig. 3A illustrates the correlations of zonal mean temperature from 5-40 km over 90°S-90°N obtained from the RO data with CPT. Fig. 3B shows the correlations of zonal mean temperature and the residual CPT after removing all variance captured by the MLR in Fig. 2.

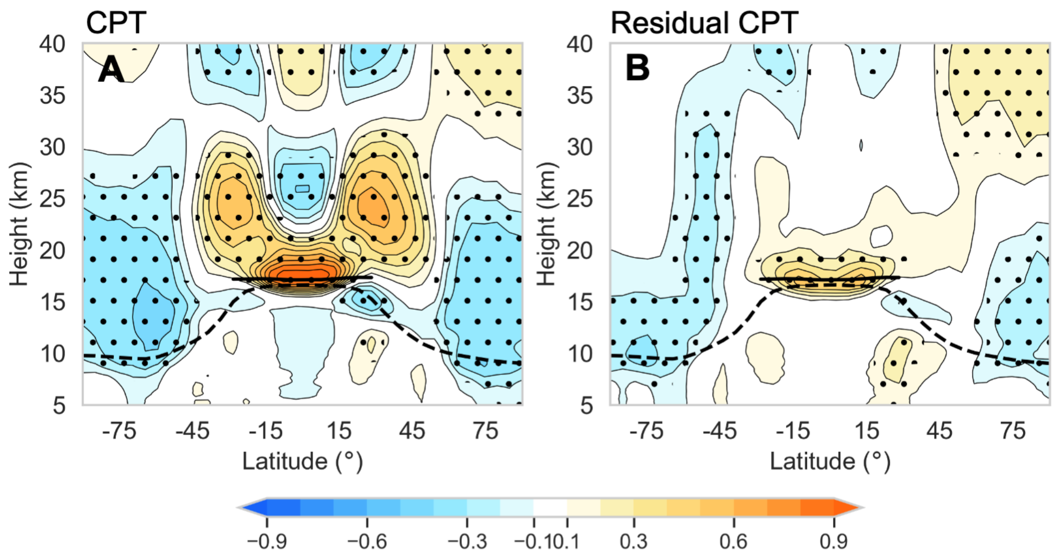

Figure 3: Correlation of zonal mean temperature globally from 5-40 km with (A) cold point temperature averaged over 15°S-15°N (CPT), and (B) residual CPT after regressing out all modes of large-scale variability using the MLR shown in Fig. 2. Stippling indicates significance at 95% confidence and the solid (dashed) black line is the climatological mean cold point (lapse rate) tropopause.

CPT is strongly correlated with temperatures throughout the global stratosphere, but not with those of the troposphere, as seen in Fig. 3A, consistent with the dominant role of stratospheric processes in CPT variance. The checkerboard pattern in the tropical stratosphere is due to the QBO's meridional circulation (Baldwin et al., 2001). The out of phase correlation above the equatorial cold point and the polar lower stratosphere is due to the BDC's meridional circulation. Regressing the modes of large-scale variability out of the CPT significantly reduces its covariability with stratospheric temperatures (Fig. 3B).

Fig. 3B shows that residual CPT is still correlated (anticorrelated) near the equatorial tropopause (polar lower stratosphere). This correlation pattern with the residual CPT is reminiscent of the global correlations expected from the BDC, which is surprising given that the QBO, BDC_{EHF}, BDC_{PSB}, T500, and MJO have all been regressed out. Note that both the CPT variability and that of zonal mean temperature throughout the global upper troposphere and lower stratosphere are derived from RO data, whereas the BDC_{EHF} and BDC_{PSB} indices are derived from ERA5 (see Section 2.2). Thus, this pattern of residual variability may be partly caused by reanalysis errors in representation of the BDC.

Figure 4 shows the correlations between zonal mean temperature with CPZ. In contrast to CPT, the CPZ is also highly correlated with temperature in the tropical troposphere (Fig. 4A). Increased tropospheric temperatures raise CPZ through thermal expansion of the troposphere in addition to dynamical upwelling. T500 contributes to nearly half of the interannual variance in CPZ (see Fig. 2), which is relevant for future increases in the CPZ in response to the T500 increase (Santer et al., 2003; Lorenz and DeWeaver, 2007). The stark differences in correlation patterns of CPT versus that of CPZ (Fig. 3A and 4A) may help validate model representations of tropical tropopause characteristics. After regressing out all modes of variability from CPZ the correlation patterns with temperature are still connected to the global stratosphere (Fig. 4B), which again indicates a potential issue in the indices used to represent the stratospheric processes.

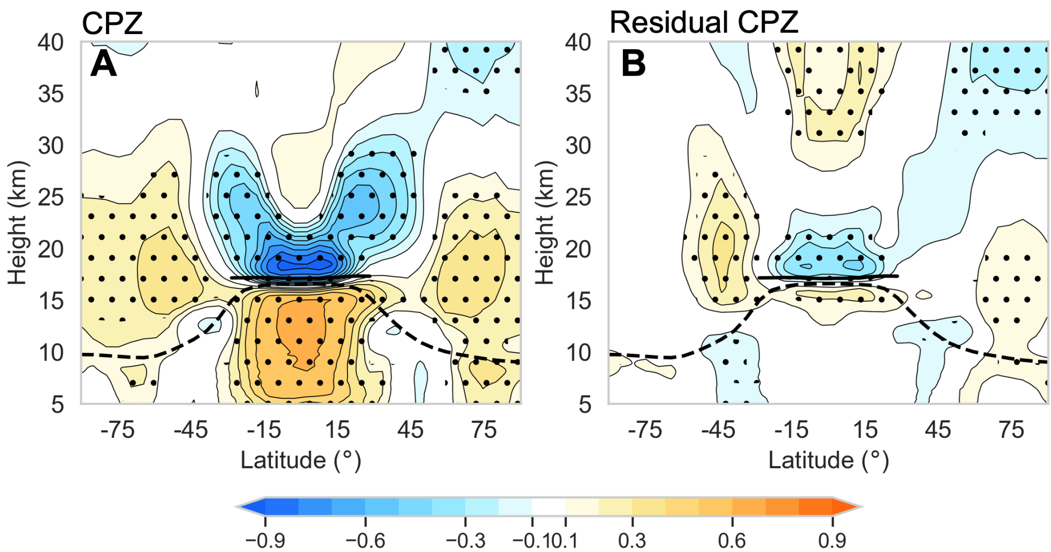

Figure 4: Same as Fig. 3, but for cold point tropopause height (CPZ).

3.3 Isolating the Role of the TTL Upwelling and Thermodynamics

The large-scale modes used as predictors in this study can impact TTL variability by modulating the TTL upwelling. This upwelling helps shape temperatures of the region through adiabatic cooling and, to a smaller extent, cloud formation and the transport of radiatively active species (Corti et al., 2006; Abalos et al., 2012; Birner and Charlesworth, 2017). On the other hand, T500 could also impact the TTL through thermodynamic processes in addition to upwelling. Here we examine the role of the dynamic upwelling and thermodynamic processes.

To assess the upwelling's impact on TTL variability, we use the original 100 hPa TEM upwelling from 15°S-15°N as described in Section 2.2. Correlations between this index and the target variables are shown in Figures 5A-E. The 100 hPa upwelling is positively correlated with tropospheric temperatures and negatively correlated with lower-stratospheric temperatures (Fig. 5A). The 100 hPa upwelling is strongly anticorrelated with CPT ($r=-0.68$) and is also anticorrelated with TTL water vapor (Fig. 5B). Upwelling also increases cloud fractions (Figs. 5D and 5E), mediated by the reductions in near tropopause temperature and vertical temperature gradient (Figs. 5A and 5C). TTLCCF has a correlation with the 100 hPa upwelling of $r=0.69$. Thus, regressing only this upwelling onto TTLCCF can explain 47% of the variability, close to what the MLR with all predictors can (52% shown in Fig. 2). Since most of the TTLCCF variance captured by the full MLR is explained using just the 100 hPa upwelling, it is suggested that the modes of the large-scale variability control TTL cirrus clouds by modulating the 100 hPa upwelling.

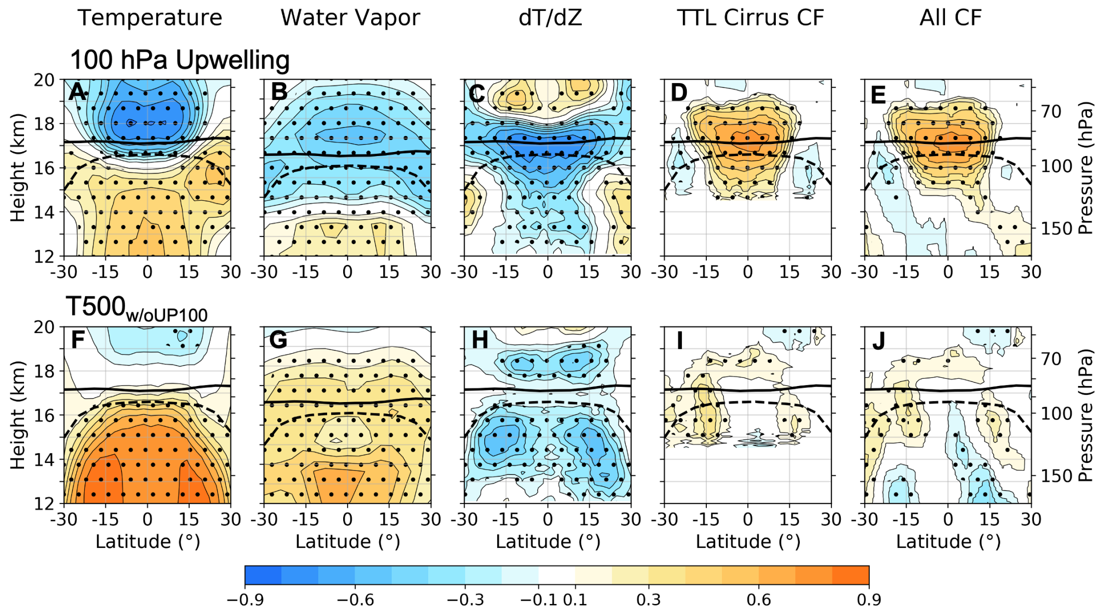

Figure 5: As Fig. 2 but A-E show correlations of target variables with the 100 hPa upwelling. F-J shows correlations with $T500_{w/oUP100}$ (i.e., T500 after regressing out the 100 hPa upwelling, QBO, and BDC_{EHF}).

Temperature and 100 hPa upwelling correlations in Fig. 5A are reminiscent of temperature and T500 correlations shown in Fig. 1U, but with stronger (weaker) correlations in stratosphere (troposphere). T500 is well correlated with the 100 hPa upwelling (r=0.49) and can influence the target variables by modulating the upwelling. T500 may induce upwelling through eddy momentum flux convergence in the tropical upper troposphere driven by convective latent heating (Boehm and Lee, 2003). However, T500 may also impact the target variables through thermodynamic processes such as radiative heating of the TTL, tropical tropospheric expansion, tropical convection, and/or other physical processes (Lin et al., 2017). We next attempt to isolate the T500 thermodynamic effects using regression analysis. It might be difficult to do so by just using the regression analysis given that the dynamic and thermodynamic processes may be closely coupled, yet this analysis may still provide valuable insights. We urge further modelling studies to validate results shown here.

To remove T500's dynamic contribution to TTL variability, we regress the 100 hPa upwelling out of T500. In addition to the 100 hPa upwelling, the QBO and BDC_{EHF} indices are also removed from T500. Since the impact of removing the QBO and BDC_{EHF} is small due to minimal correlations with T500 (Fig. S3), we refer to this T500 index without the dynamic components as $T500_{w/oUP100}$(which can be considered as the T500 thermodynamic index). Figures 5F-J show the correlation coefficients between $T500_{w/oUP100}$ with target variables. Fig. 5F shows warming below the tropopause and little to no cooling in the stratosphere as would be expected after removing the dynamically induced response to T500. While significant positive tropospheric temperature correlations in Fig. 5F reach closer to the equatorial cold point tropopause than those with the original T500 index shown in Fig. 1U, no statistically significant correlation between $T500_{w/oUP100}$ and CPT exists (r=0.15). Given that the 100 hPa upwelling explains most of the TTLCCF variability, removing its influence from T500 also largely removes its influence on TTL cirrus clouds (Figs. 5I and 5J).

Notably, $T500_{w/oUP100}$ shows a significant correlation with lower-stratospheric water vapor (Fig. 5G). This is in stark contrast to results of Fig. 1V, where the T500 index showed no significant impact on lower-stratospheric water vapor. Fig. 5G may suggest that $T500_{w/oUP100}$ covaries with lower-stratospheric water vapor, but this covariability is damped by coincident cooling due to the TTL upwelling caused by T500. While $T500_{w/oUP100}$ is correlated with lower-stratospheric water vapor, it is not significantly correlated with CPT. Thus, the $T500_{w/oUP100}$ impact on lower-stratospheric water vapor might not work through a simple increase in CPT but may instead be related to $T500_{w/oUP100}$'s impact on the TTL environment where dehydration, convective evaporation, subtropical water vapor in-mixing, and/or other uninvestigated processes occur (Dessler et al., 2013; Ye et al., 2018; Bourguet and Linz, 2023).

The differences between Figs. 1U-Y and Figs. 5F-J suggest that T500 contributes to TTL variability partly through changes in the 100 hPa upwelling. Figure 6 is the same as Fig. 2 but replaces T500 with $T500_{w/oUP100}$ and BDC_{PSB} with BDC_{PSB}+$UP100_{T500}$. BDC_{PSB}+$UP100_{T500}$ is the combination of BDC_{PSB} and the 100 hPa upwelling induced by T500, which is computed in the same way as BDC_{PSB} but without regressing out T500 (see Section 2.2). This replacement is to group the T500 that is linearly related to the 100 hPa upwelling ($UP100_{T500}$) with the BDC_{PSB} and then isolate the T500 that is not linearly related to the 100 hPa upwelling ($T500_{w/oUP100}$).

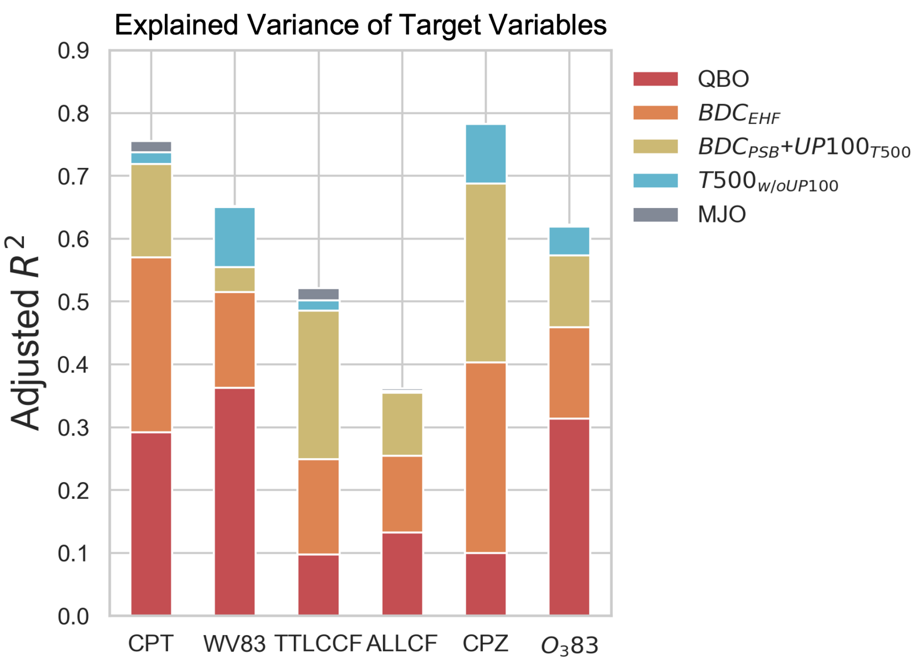

Figure 6: Same as Fig. 2, but the BDC_{PSB}+$UP100_{T500}$ is the BDC_{PSB} without removing the influence of T500, i.e., the contribution from BDC_{PSB} and the 100 hPa upwelling due to T500 ($UP100_{T500}$). $T500_{w/oUP100}$ is the T500 index after regressing out the original 100 hPa upwelling, the QBO, and BDC.

This replacement does not impact the total explained variance, and small changes in explained variances by QBO, BDC_{EHF} and MJO result from changes in collinearities. Figure 6 shows that $T500_{w/oUP100}$ contributes minimally to explained variance of TTLCCF and ALLCF because cloud fraction variance is tightly coupled to the TTL upwelling. While Fig. 2 showed that T500 contributes nearly half of the explained variance in CPZ, Fig. 6 shows that $T500_{w/oUP100}$ contributes much less to the explained variance in CPZ. Figures 2 and 6 suggest that more than 2/3 of the T500 control of CPZ is through T500's induced upwelling (Austin and Reichler, 2008). Similarly, only about 1/3 of explained $O_3$83 variance by T500 (Fig.2) comes from $T500_{w/oUP100}$ (Fig.6).

In contrast, Fig. 6 shows an enhanced role of $T500_{w/oUP100}$ in WV83 variance relative to T500 in Fig. 2. The $T500_{w/oUP100}$ influence on WV83 may be important for climate feedbacks due to the important role of lower-stratospheric water vapor (Solomon et al., 2010). Finally it is worth noting that the explained CPT variances by BDC_{PSB} (Fig.2) and BDC_{PSB}+$UP100_{T500}$ (Fig. 6) are almost identical, indicating that both $UP100_{T500}$ and $T500_{w/oUP100}$ have little impacts on CPT.

3.4 Seasonality

The seasonal influence of large-scale modes on TTL variability is less studied. Correlation between CPT and lower-stratospheric water vapor is strongest in boreal winter (Randel and Jensen, 2013; Randel and Park, 2019; Lu et al., 2020). Seasonal changes in the tropical upwelling and the Asian monsoon also impact TTL variability (Sunilkumar et al., 2010; Randel et al., 2007; Randel et al 2010; Walker et al., 2015; Ueyama et al., 2015; Ueyama et al., 2018; Das and Suneeth, 2020). Modes of the large-scale variability may also impact the target variables differently throughout the year (Li and Thompson, 2013; Konopka et al., 2016; Tweedy et al., 2018; Martin et al., 2021; Sweeney et al., 2023). Here, we examine how these modes of variability impact the target variables during extended boreal winter (November-March; NDJFM) and extended boreal summer (May-September; MJJAS). During NDJFM the TTL is colder, drier, and has more TTL cirrus than in MJJAS (Figure S4). During MJJAS, lower stratospheric water vapor increases (Fig. S4G) and All cloud fraction maximizes (Fig. S4J) in the northern hemisphere TTL due to the Asian Summer Monsoon (e.g., Santee et al., 2017). Regardless of season, interannual variance is strongest near the equator (Fig. S4).

The MLR used in Fig. 2 is fit in both NDJFM and MJJAS individually in Figure 7. Figure S5 shows correlation matrices between all target variables and predictors for both NDJFM and MJJAS separately. The MLR predicts all target variables better during NDFJM than MJJAS, except ALLCF. Note that the partitioning of explained variance is less reliable after splitting the data based on season because of collinearities between the modes of variability, and smaller number of degrees of freedom.

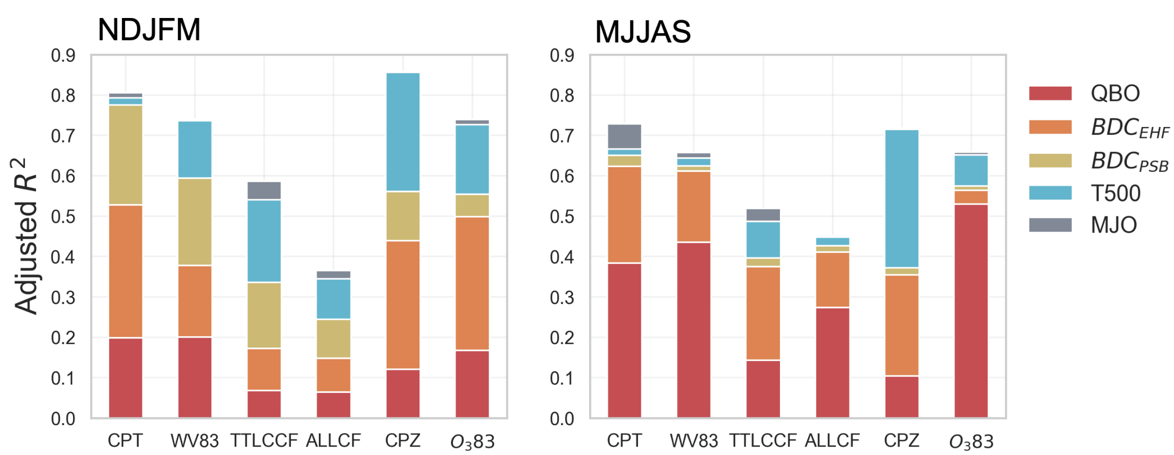

Figure 7: Adjusted R^2 from MLR model applied to target variables for NDJFM and MJJAS individually. Colored sections indicate the contribution to the adjusted R^2 from each predictor.

Fig. 7 highlights the increased QBO influence during MJJAS for all variables except CPZ: CPT (r=0.5 in NDJFM and r=0.61 in MJJAS), WV83 (0.53 in NDJFM and 0.66 in MJJAS), TTLCCF (r=-0.26 in NDJFM and r=-0.36 in MJJAS), ALLCF (r=-0.26 in NDJFM and -0.51 in MJJAS), and $O_3$83 (r=0.43 in NDJFM and r=0.72 in MJJAS). This is despite the stronger QBO-MJO connection and lower-stratospheric temperature impact during boreal winter (Yoo and Son, 2016; Tegtmeier et al., 2020; Martin et al., 2021). A seasonality in the QBO's descent has been well documented (Dunkerton, 1990; Coy et al., 2020). Seasonal changes in the QBO's explained variance may be a result of a seasonality in the zonal symmetry of the QBO impact on the TTL (Tegtmeier et al., 2020). The MJJAS TTL is less variable than that of NDJFM (compare rows 3 and 4 of Fig. S4), so an equally large QBO signal should be more salient during this season.

The BDC_{EHF} TTL impact maximizes during boreal winter due to increased extratropical stratospheric wave driving (Yulaeva, et al., 1994). NDJFM BDC_{EHF} impacts are larger for CPT, CPZ, and $O_3$83. The BDC_{EHF} impact on WV83 is comparable during both seasons, but this result is complicated by the strength of the BDC_{EHF} during the two seasons and thus the time of transit between the CPT and 83 hPa (Randel and Park, 2019). WV83 results of Fig. 7 are lagged by one-month (see section 2.1). Removing this one-month lag reveals the much stronger BDC_{EHF} control of WV83 during NDJFM compared to MJJAS. We find that the BDC_{EHF} explanation of TTL cirrus clouds is larger during MJJAS (correlation between BDC and TTLCCF is r=0.39 in NDJFM and r=0.51 in MJJAS). This is surprising given the strong connections between the boreal winter BDC_{EHF} and TTL cirrus clouds previously reported (Li and Thompson, 2013), but is not studied further here. Increased explained variance of target variables during NDFJM is partly due to the role of BDC_{PSB}. Although the seasonal cycle in the BDC_{PSB} index has been removed, anomalies are weaker during MJJAS. This may be related to stronger subtropical wave driving variability during NDJFM (Randel et al., 2008; Ortland and Alexander, 2014).

T500's impact on the target variables is stronger in NDJFM for WV83, TTLCCF, ALLCF, and $O_3$83. This increase in the tropospheric influence on the TTL variability during these seasons may be related to seasonality in ENSO activity or tropical wave activity captured by the T500 index (Ortland and Alexander, 2014; Garfinkel et al., 2018). The seasonality of the MJO impact on the target variables is more inconsistent and may be further complicated due to aliasing of the Boreal Summer Intraseasonal Oscillation into our MJO index.

4 Discussion and Conclusions

Stratospheric water vapor and TTL cirrus clouds are important components of the climate system but poorly constrained in models. Both exhibit large interannual variability and are linked by temperature in the TTL (Jensen et al., 2013; Tseng and Fu, 2017a). The QBO, BDC_{EHF}, BDC_{PSB}, T500, and MJO contribute to this interannual variability by modulating the dynamic and thermodynamic environment of the TTL (e.g., Dessler et al., 2013; Davis et al., 2013; Randel and Wu, 2015). Multiple linear regressions (MLRs) with modes of the large-scale variability as predictors have been used to study the temperature control of water vapor and TTL cirrus clouds (Dessler et al., 2014; Austin and Reichler, 2008; Oman et al., 2008; Garfinkel et al., 2018). Here we synthesize these results by applying a MLR to CPT, WV83, and TTLCCF and further previous efforts by applying the MLR to ALLCF, CPZ, and $O_3$83.

The MLR explains significant amounts of variance in CPT (76%), WV83 (65%), TTLCCF (52%), ALLCF (36%), CPZ (78%), and $O_3$83 (62%). Decomposing the explained variance by predictor reveals that for all variables the stratospheric processes explain a larger fraction of the variance. A strong stratospheric predictor of the target variables which received little attention in previous studies is BDC_{PSB}. Temperature and BDC_{PSB} correlations have a distinct pattern (see Fig. 1P) reminiscent of temperature tendencies caused by subtropical wave driving (Randel et al., 2008; Grise and Thompson, 2013; Abalos et al., 2014). Future work should identify the source of variability of BDC_{PSB}, as it is a significant source of TTL variability. To our knowledge, this is also the first study to show the observed connection between the tropical cold point tropopause temperature and height and global tropospheric and stratospheric temperatures.

Nearly all explained CPT variability comes from the QBO, BDC_{EHF}, and BDC_{PSB} (see Fig. 2). Notably, CPT is not correlated with tropical tropospheric temperatures (Fig. 3A). In contrast CPZ is controlled by near equal contributions from stratospheric and tropospheric processes. The robust correlation between CPT (CPZ) and stratospheric (stratospheric and tropospheric) temperatures shown in Fig. 3A (Fig. 4A) can be used to validate model representations of tropopause characteristics. GCM simulations suggest that CPZ and CPT increase in response to warming (Austin and Reichler, 2008; Gettelman et al., 2009; Gettelman et al., 2010; Hardiman et al., 2015; Lin et al., 2017; Wang and Fu, 2023). To the extent that interannual responses to T500 increases can be compared with model simulations of surface warming, observed interannual variability is consistent with model simulations for the CPZ response to tropospheric warming, but not for the CPT response (Lin et al., 2017).

T500 can dynamically induce TTL upwelling. However, T500 can also impact the TTL through thermodynamic processes not directly tied to the upwelling (Lin et al., 2017; Ye et al., 2018; Bourguet and Linz, 2023). To isolate the dynamical impact of T500, the T500 index was separated into the part that was linearly related to the 100 hPa upwelling and that which was not. Our results suggest that the primary influence of T500 on TTLCCF, ALLCF, CPZ and $O_3$83 is via the dynamically induced upwelling (comparing Figs. 6 and 2). Notably, the T500 index that is independent of the TTL upwelling is significantly correlated with lower-stratospheric water vapor (Fig. 5G) which may be relevant for climate feedbacks (Dessler et al., 2013). While T500 is expected to increase with greenhouse gas concentrations, its interannual variability is greatly influenced by ENSO that is associated with specific SST pattern changes, and thus conclusions relevant to climate change drawn from the results shown here need to be validated by modeling studies.

Because of the CPT's central role in stratospheric water vapor and TTL cloud fraction, it is critically important to understand its interannual variability. The correlation patterns between temperature and residual CPT (after regressing out all modes of variability) still resemble the BDC, with positive (negative) correlations near the tropical (polar) lower stratosphere (Fig. 3B). Given that we regressed out both the BDC_{EHF} and BDC_{PSB} indices, this residual CPT correlation resembling the BDC is surprising. Zonal mean temperature data and the CPT timeseries used in Fig. 3A comes from RO observations, whereas the BDC_{EHF} and BDC_{PSB} indices come from ERA5, and thus the residual correlation pattern may result from the tropical upwelling quantification from reanalysis. The residual variability in WV83 and $O_3$83 is also correlated with the global stratosphere (Figure S6). Future work should thus aim to better understand this dynamical influence of the stratospheric circulation on the CPT.

Acknowledgments

This research is supported by the NASA FINESST Grant 80NSSC22K1438 and NSF Grant AGS-2202812. Additional funding was provided by the Calvin Professorship in Atmospheric Sciences. We thank Prof. John M. Wallace and Mingcheng Wang for their valuable discussions regarding the paper. We also thank the two anonymous reviewers for their help in shaping the scope of the paper, and Stephen Bourguet for his insight and thoughtful comments which were critical to the final version of the paper.

Open Research

The data on which this article is based are available in Sweeney and Fu., 2023. Software required to recreate the results is provided in Sweeney (2023).

References

Abalos, M., Randel, W. J., & Serrano, E. (2012). Variability in upwelling across the tropical tropopause and correlations with tracers in the lower stratosphere. *Atmospheric Chemistry and Physics*, *12*(23), 11505–11517. https://doi.org/10.5194/acp-12-11505-2012

Abalos, Marta, Randel, W. J., & Serrano, E. (2014). Dynamical Forcing of Subseasonal Variability in the Tropical Brewer–Dobson Circulation. *Journal of the Atmospheric Sciences*, *71*(9), 3439–3453. https://doi.org/10.1175/JAS-D-13-0366.1

Anthes, R. A., Bernhardt, P. A., Chen, Y., Cucurull, L., Dymond, K. F., Ector, D., et al. (2008). The COSMIC/FORMOSAT-3 Mission: Early Results. *Bulletin of the American Meteorological Society*, *89*(3), 313–334. https://doi.org/10.1175/BAMS-89-3-313

Austin, J., & Reichler, T. J. (2008). Long-term evolution of the cold point tropical tropopause: Simulation results and attribution analysis. *Journal of Geophysical Research: Atmospheres*, *113*(D7). https://doi.org/10.1029/2007JD009768

Avery, M. A., Davis, S. M., Rosenlof, K. H., Ye, H., & Dessler, A. E. (2017). Large anomalies in lower stratospheric water vapour and ice during the 2015–2016 El Niño. *Nature Geoscience*, *10*(6), 405–409. https://doi.org/10.1038/ngeo2961

Baldwin, M. P., Gray, L. J., Dunkerton, T. J., Hamilton, K., Haynes, P. H., Randel, W. J., et al. (2001). The quasi-biennial oscillation. *Reviews of Geophysics*, *39*(2), 179–229. https://doi.org/10.1029/1999RG000073

Banerjee, A., Maycock, A. C., Archibald, A. T., Abraham, N. L., Telford, P., Braesicke, P., & Pyle, J. A. (2016). Drivers of changes in stratospheric and tropospheric ozone between year 2000 and 2100. *Atmospheric Chemistry and Physics*, *16*(5), 2727–2746. https://doi.org/10.5194/acp-16-2727-2016

Birner, T., & Charlesworth, E. J. (2017). On the relative importance of radiative and dynamical heating for tropical tropopause temperatures. *Journal of Geophysical Research: Atmospheres*, *122*(13), 6782–6797. https://doi.org/10.1002/2016JD026445

Boehm, M. T., & Lee, S. (2003). The Implications of Tropical Rossby Waves for Tropical Tropopause Cirrus Formation and for the Equatorial Upwelling of the Brewer–Dobson Circulation. *Journal of the Atmospheric Sciences*, *60*(2), 247–261. https://doi.org/10.1175/1520-0469(2003)060<0247:TIOTRW>2.0.CO;2

Boehm, M. T., & Verlinde, J. (2000). Stratospheric influence on upper tropospheric tropical cirrus. *Geophysical Research Letters*, *27*(19), 3209–3212. https://doi.org/10.1029/2000GL011678

Bourguet, S., & Linz, M. (2023). Weakening of the tropical tropopause layer cold trap with global warming. *Atmospheric Chemistry and Physics*, *23*(13), 7447–7460. https://doi.org/10.5194/acp-23-7447-2023

Bramberger, M., Alexander, M. J., Davis, S., Podglajen, A., Hertzog, A., Kalnajs, L., et al. (2022). First Super-Pressure Balloon-Borne Fine-Vertical-Scale Profiles in the Upper TTL:

Impacts of Atmospheric Waves on Cirrus Clouds and the QBO. *Geophysical Research Letters*, *49*(5), e2021GL097596. https://doi.org/10.1029/2021GL097596

Brewer, A. W. (1949). Evidence for a world circulation provided by the measurements of helium and water vapour distribution in the stratosphere. *Quarterly Journal of the Royal Meteorological Society*, *75*(326), 351–363. https://doi.org/10.1002/qj.49707532603

Butchart, N., Anstey, J. A., Kawatani, Y., Osprey, S. M., Richter, J. H., & Wu, T. (2020). QBO Changes in CMIP6 Climate Projections. *Geophysical Research Letters*, *47*(7), e2019GL086903. https://doi.org/10.1029/2019GL086903

Calvo, N., Garcia, R. R., Randel, W. J., & Marsh, D. R. (2010). Dynamical Mechanism for the Increase in Tropical Upwelling in the Lowermost Tropical Stratosphere during Warm ENSO Events. *Journal of the Atmospheric Sciences*, *67*(7), 2331–2340. https://doi.org/10.1175/2010JAS3433.1

Chang, K.-W., & L'Ecuyer, T. (2020). Influence of gravity wave temperature anomalies and their vertical gradients on cirrus clouds in the tropical tropopause layer – a satellite-based view. *Atmospheric Chemistry and Physics*, *20*(21), 12499–12514. https://doi.org/10.5194/acp-20-12499-2020

Charlesworth, E. J., Birner, T., & Albers, J. R. (2019). Ozone Transport-Radiation Feedbacks in the Tropical Tropopause Layer. *Geophysical Research Letters*, *46*(23), 14195–14202. https://doi.org/10.1029/2019GL084679

Chiodo, G., Polvani, L. M., Marsh, D. R., Stenke, A., Ball, W., Rozanov, E., et al. (2018). The Response of the Ozone Layer to Quadrupled CO2 Concentrations. *Journal of Climate*, *31*(10), 3893–3907. https://doi.org/10.1175/JCLI-D-17-0492.1

Corti, T., Luo, B. P., Fu, Q., Vomel, H., & Peter, T. (2006). The impact of cirrus clouds on tropical troposphere-to-stratosphere transport. *Atmos. Chem. Phys.*, 9.

Coy, L., Newman, P. A., Strahan, S., & Pawson, S. (2020). Seasonal Variation of the Quasi-Biennial Oscillation Descent. *Journal of Geophysical Research: Atmospheres*, *125*(18), e2020JD033077. https://doi.org/10.1029/2020JD033077

Das, S. S., & Suneeth, K. V. (2020). Seasonal and interannual variations of water vapor in the upper troposphere and lower stratosphere over the Asian Summer Monsoon region- in perspective of the tropopause and ocean-atmosphere interactions. *Journal of Atmospheric and Solar-Terrestrial Physics*, *201*, 105244. https://doi.org/10.1016/j.jastp.2020.105244

Davis, S. M., Liang, C. K., & Rosenlof, K. H. (2013). Interannual variability of tropical tropopause layer clouds. *Geophysical Research Letters*, *40*(11), 2862–2866. https://doi.org/10.1002/grl.50512

Deckert, R., & Dameris, M. (2008). Higher tropical SSTs strengthen the tropical upwelling via deep convection. *Geophysical Research Letters*, *35*(10). https://doi.org/10.1029/2008GL033719

Dessler, A. E., Schoeberl, M. R., Wang, T., Davis, S. M., & Rosenlof, K. H. (2013). Stratospheric water vapor feedback. *Proceedings of the National Academy of Sciences*, *110*(45), 18087–18091. https://doi.org/10.1073/pnas.1310344110

Dessler, A. E., Schoeberl, M. R., Wang, T., Davis, S. M., Rosenlof, K. H., & Vernier, J.-P. (2014). Variations of stratospheric water vapor over the past three decades. *Journal of Geophysical Research: Atmospheres*, *119*(22), 12,588-12,598. https://doi.org/10.1002/2014JD021712

Diallo, M., Riese, M., Birner, T., Konopka, P., Müller, R., Hegglin, M. I., et al. (2018). Response of stratospheric water vapor and ozone to the unusual timing of El Niño and the QBO disruption in 2015–2016. *Atmospheric Chemistry and Physics*, *18*(17), 13055–13073. https://doi.org/10.5194/acp-18-13055-2018

Ding, Q., & Fu, Q. (2018). A warming tropical central Pacific dries the lower stratosphere. *Climate Dynamics*, *50*(7), 2813–2827. https://doi.org/10.1007/s00382-017-3774-y

Dinh, T. P., Durran, D. R., & Ackerman, T. P. (2010). Maintenance of tropical tropopause layer cirrus. *Journal of Geophysical Research: Atmospheres*, *115*(D2). https://doi.org/10.1029/2009JD012735

Dunkerton, T. (1990). Annual variation of deseasonalized mean flow acceleration in the equatorial lower stratosphere. https://doi.org/10.2151/JMSJ1965.68.4_499

Eguchi, N., & Kodera, K. (2010). Impacts of Stratospheric Sudden Warming Event on Tropical Clouds and Moisture Fields in the TTL: A Case Study. *Sola*, *6*, 137–140. https://doi.org/10.2151/sola.2010-035

de F. Forster, P. M., & Shine, K. P. (1999). Stratospheric water vapour changes as a possible contributor to observed stratospheric cooling. *Geophysical Research Letters*, *26*(21), 3309–3312. https://doi.org/10.1029/1999GL010487

Flury, T., Wu, D. L., & Read, W. G. (2012). Correlation among cirrus ice content, water vapor and temperature in the TTL as observed by CALIPSO and Aura/MLS. *Atmospheric Chemistry and Physics*, *12*(2), 683–691. https://doi.org/10.5194/acp-12-683-2012

Flury, Thomas, wu, D., & Read, W. (2012). Variability of the Brewer-Dobson circulation's meridional and vertical branch using Aura/MLS water vapor. *Atmospheric Chemistry & Physics Discussions*, *12*, 21291–21320. https://doi.org/10.5194/acpd-12-21291-2012

Fu, Q., Lin, P., Solomon, S., & Hartmann, D. L. (2015). Observational evidence of strengthening of the Brewer-Dobson circulation since 1980. *Journal of Geophysical Research: Atmospheres*, *120*(19), 10,214-10,228. https://doi.org/10.1002/2015JD023657

Fu, Qiang. (2013). Bottom up in the tropics. *Nature Climate Change*, *3*(11), 957–958. https://doi.org/10.1038/nclimate2039

Fu, Qiang, Hu, Y., & Yang, Q. (2007). Identifying the top of the tropical tropopause layer from vertical mass flux analysis and CALIPSO lidar cloud observations. *Geophysical Research Letters*, *34*(14). https://doi.org/10.1029/2007GL030099

Fu, Qiang, Smith, M., & Yang, Q. (2018). The Impact of Cloud Radiative Effects on the Tropical Tropopause Layer Temperatures. *Atmosphere*, *9*(10), 377. https://doi.org/10.3390/atmos9100377

Fueglistaler, S., & Haynes, P. H. (2005). Control of interannual and longer-term variability of stratospheric water vapor. *Journal of Geophysical Research: Atmospheres*, *110*(D24). https://doi.org/10.1029/2005JD006019

Fueglistaler, S., Dessler, A. E., Dunkerton, T. J., Folkins, I., Fu, Q., & Mote, P. W. (2009). Tropical tropopause layer. *Reviews of Geophysics*, *47*(1). https://doi.org/10.1029/2008RG000267

Garcia, R. R., & Randel, W. J. (2008). Acceleration of the Brewer–Dobson Circulation due to Increases in Greenhouse Gases. *Journal of the Atmospheric Sciences*, *65*(8), 2731–2739. https://doi.org/10.1175/2008JAS2712.1

Garfinkel, C. I., & Hartmann, D. L. (2008). Different ENSO teleconnections and their effects on the stratospheric polar vortex. *Journal of Geophysical Research: Atmospheres*, *113*(D18). https://doi.org/10.1029/2008JD009920

Garfinkel, C. I., Waugh, D. W., Oman, L. D., Wang, L., & Hurwitz, M. M. (2013). Temperature trends in the tropical upper troposphere and lower stratosphere: Connections with sea surface temperatures and implications for water vapor and ozone. *Journal of Geophysical Research: Atmospheres*, *118*(17), 9658–9672. https://doi.org/10.1002/jgrd.50772

Garfinkel, Chaim I, Gordon, A., Oman, L. D., Li, F., Davis, S., & Pawson, S. (2018). Nonlinear response of tropical lower stratospheric temperature and water vapor to ENSO. *Atmospheric Chemistry and Physics*, *18*(7), 4597–4615. https://doi.org/10.5194/acp-18-4597-2018

Garfinkel, Chaim I., Harari, O., Ziskin Ziv, S., Rao, J., Morgenstern, O., Zeng, G., et al. (2021). Influence of the El Niño–Southern Oscillation on entry stratospheric water vapor in coupled chemistry–ocean CCMI and CMIP6 models. *Atmospheric Chemistry and Physics*, *21*(5), 3725–3740. https://doi.org/10.5194/acp-21-3725-2021

Garny, H., Dameris, M., Randel, W., Bodeker, G. E., & Deckert, R. (2011). Dynamically Forced Increase of Tropical Upwelling in the Lower Stratosphere. *Journal of the Atmospheric Sciences*, *68*(6), 1214–1233. https://doi.org/10.1175/2011JAS3701.1

GetTELman, A., & Forster, P. M. de F. (2002). A Climatology of the Tropical Tropopause Layer. *Journal of the Meteorological Society of Japan. Ser. II*, *80*(4B), 911–924. https://doi.org/10.2151/jmsj.80.911

Gettelman, A., Birner, T., Eyring, V., Akiyoshi, H., Bekki, S., Brühl, C., et al. (2009). The Tropical Tropopause Layer 1960–2100. *Atmospheric Chemistry and Physics*, *9*(5), 1621–1637. https://doi.org/10.5194/acp-9-1621-2009

Gettelman, A., Hegglin, M. I., Son, S.-W., Kim, J., Fujiwara, M., Birner, T., et al. (2010). Multimodel assessment of the upper troposphere and lower stratosphere: Tropics and global trends. *Journal of Geophysical Research: Atmospheres*, *115*(D3). https://doi.org/10.1029/2009JD013638

Gettelman, Andrew, Forster, P. M. de F., Fujiwara, M., Fu, Q., Vömel, H., Gohar, L. K., et al. (2004). Radiation balance of the tropical tropopause layer. *Journal of Geophysical Research: Atmospheres*, *109*(D7). https://doi.org/10.1029/2003JD004190

Grise, K. M., & Thompson, D. W. J. (2013). On the Signatures of Equatorial and Extratropical Wave Forcing in Tropical Tropopause Layer Temperatures. *Journal of the Atmospheric Sciences*, *70*(4), 1084–1102. https://doi.org/10.1175/JAS-D-12-0163.1

Hardiman, S. C., Boutle, I. A., Bushell, A. C., Butchart, N., Cullen, M. J. P., Field, P. R., et al. (2015). Processes Controlling Tropical Tropopause Temperature and Stratospheric Water Vapor in Climate Models. *Journal of Climate*, *28*(16), 6516–6535. https://doi.org/10.1175/JCLI-D-15-0075.1

Haynes, P. H., McIntyre, M. E., Shepherd, T. G., Marks, C. J., & Shine, K. P. (1991). On the "Downward Control" of Extratropical Diabatic Circulations by Eddy-Induced Mean Zonal Forces. *Journal of the Atmospheric Sciences*, *48*(4), 651–678. https://doi.org/10.1175/1520-0469(1991)048<0651:OTCOED>2.0.CO;2

Hersbach, H., Bell, B., Berrisford, P., Hirahara, S., Horányi, A., Muñoz-Sabater, J., et al. (2020). The ERA5 global reanalysis. *Quarterly Journal of the Royal Meteorological Society*, *146*(730), 1999–2049. https://doi.org/10.1002/qj.3803

Holton, J., & Gettelman, A. (2001). Horizontal transport and dehydration in the stratosphere. *Geophys. Res. Lett.*, *28*, 2799–2802. https://doi.org/10.1029/2001GL013148

Holton, J., Haynes, P., Mcintyre, M., Douglass, A., Rood, R., & Pfister, L. (1995). Stratosphere-Troposphere Exchange. *Reviews of Geophysics - REV GEOPHYS*, *33*. https://doi.org/10.1029/95RG02097

Jensen, E. J., Toon, O. B., Pfister, L., & Selkirk, H. B. (1996). Dehydration of the upper troposphere and lower stratosphere by subvisible cirrus clouds near the tropical tropopause. *Geophysical Research Letters*, *23*(8), 825–828. https://doi.org/10.1029/96GL00722

Jensen, E. J., Diskin, G., Lawson, R. P., Lance, S., Bui, T. P., Hlavka, D., et al. (2013). Ice nucleation and dehydration in the Tropical Tropopause Layer. *Proceedings of the National Academy of Sciences*, *110*(6), 2041–2046. https://doi.org/10.1073/pnas.1217104110

Joshi, M. M., Webb, M. J., Maycock, A. C., & Collins, M. (2010). Stratospheric water vapour and high climate sensitivity in a version of the HadSM3 climate model. *Atmospheric Chemistry and Physics*, *10*(15), 7161–7167. https://doi.org/10.5194/acp-10-7161-2010

Kim, J., Randel, W. J., Birner, T., & Abalos, M. (2016). Spectrum of Wave Forcing Associated with the Annual Cycle of Upwelling at the Tropical Tropopause. *Journal of the Atmospheric Sciences*, *73*(2), 855–868. https://doi.org/10.1175/JAS-D-15-0096.1

Kim, J.-E., & Alexander, M. J. (2015). Direct impacts of waves on tropical cold point tropopause temperature. *Geophysical Research Letters*, *42*(5), 1584–1592. https://doi.org/10.1002/2014GL062737

Kim, J.-E., Alexander, M. J., Bui, T. P., Dean-Day, J. M., Lawson, R. P., Woods, S., et al. (2016). Ubiquitous influence of waves on tropical high cirrus clouds. *Geophysical Research Letters*, *43*(11), 5895–5901. https://doi.org/10.1002/2016GL069293

Kirk-Davidoff, D. B., Hintsa, E. J., Anderson, J. G., & Keith, D. W. (1999). The effect of climate change on ozone depletion through changes in stratospheric water vapour. *Nature*, *402*(6760), 399–401. https://doi.org/10.1038/46521

Konopka, P., Grooß, J.-U., Plöger, F., & Müller, R. (2009). Annual cycle of horizontal in-mixing into the lower tropical stratosphere. *Journal of Geophysical Research: Atmospheres*, *114*(D19). https://doi.org/10.1029/2009JD011955

Konopka, P., Ploeger, F., Tao, M., & Riese, M. (2016). Zonally resolved impact of ENSO on the stratospheric circulation and water vapor entry values. *Journal of Geophysical Research: Atmospheres*, *121*(19), 11,486-11,501. https://doi.org/10.1002/2015JD024698

Kuo, Y.-H., Wee, T.-K., Sokolovskiy, S., Rocken, C., Schreiner, W., Hunt, D., & Anthes, R. A. (2004). Inversion and Error Estimation of GPS Radio Occultation Data. *Journal of the Meteorological Society of Japan. Ser. II*, *82*(1B), 507–531. https://doi.org/10.2151/jmsj.2004.507

Kursinski, E. R., Hajj, G. A., Schofield, J. T., Linfield, R. P., & Hardy, K. R. (1997). Observing Earth's atmosphere with radio occultation measurements using the Global Positioning System. *Journal of Geophysical Research: Atmospheres*, *102*(D19), 23429–23465. https://doi.org/10.1029/97JD01569

Li, Y., & Thompson, D. W. J. (2013). The signature of the stratospheric Brewer–Dobson circulation in tropospheric clouds. *Journal of Geophysical Research: Atmospheres*, *118*(9), 3486–3494. https://doi.org/10.1002/jgrd.50339

Liang, C. K., Eldering, A., Gettelman, A., Tian, B., Wong, S., Fetzer, E. J., & Liou, K. N. (2011). Record of tropical interannual variability of temperature and water vapor from a combined AIRS-MLS data set. *Journal of Geophysical Research: Atmospheres*, *116*(D6). https://doi.org/10.1029/2010JD014841

Lin, P., & Fu, Q. (2013). Changes in various branches of the Brewer–Dobson circulation from an ensemble of chemistry climate models. *Journal of Geophysical Research: Atmospheres*, *118*(1), 73–84. https://doi.org/10.1029/2012JD018813

Lin, Pu, Fu, Q., Solomon, S., & Wallace, J. M. (2009). Temperature Trend Patterns in Southern Hemisphere High Latitudes: Novel Indicators of Stratospheric Change. *Journal of Climate*, *22*(23), 6325–6341. https://doi.org/10.1175/2009JCLI2971.1

Lin, Pu, Paynter, D., Ming, Y., & Ramaswamy, V. (2017). Changes of the Tropical Tropopause Layer under Global Warming. *Journal of Climate*, *30*(4), 1245–1258. https://doi.org/10.1175/JCLI-D-16-0457.1

Lindeman, R. H., Merenda, P. F., & Gold, R. Z. (1980). *Introduction to bivariate and multivariate analysis*. Glenview, Ill: Scott, Foresman.

Livesey, N. J., Read, W. G., Froidevaux, L., Lambert, A., Santee, M. L., Schwartz, M. J., et al. (2021). Investigation and amelioration of long-term instrumental drifts in water vapor and nitrous oxide measurements from the Aura Microwave Limb Sounder (MLS) and their implications for studies of variability and trends. *Atmospheric Chemistry and Physics*, *21*(20), 15409–15430. https://doi.org/10.5194/acp-21-15409-2021

Lorenz, D. J., & DeWeaver, E. T. (2007). Tropopause height and zonal wind response to global warming in the IPCC scenario integrations. *Journal of Geophysical Research: Atmospheres*, *112*(D10). https://doi.org/10.1029/2006JD008087

Lu, J., Xie, F., Sun, C., Luo, J., Cai, Q., Zhang, J., et al. (2020). Analysis of factors influencing tropical lower stratospheric water vapor during 1980–2017. *Npj Climate and Atmospheric Science*, *3*(1), 1–11. https://doi.org/10.1038/s41612-020-00138-7

Madden, R. A., & Julian, P. R. (1971). Detection of a 40–50 Day Oscillation in the Zonal Wind in the Tropical Pacific. *Journal of the Atmospheric Sciences*, *28*(5), 702–708. https://doi.org/10.1175/1520-0469(1971)028<0702:DOADOI>2.0.CO;2

Marsh, D. R., & Garcia, R. R. (2007). Attribution of decadal variability in lower-stratospheric tropical ozone. *Geophysical Research Letters*, *34*(21). https://doi.org/10.1029/2007GL030935

Martin, Z., Sobel, A., Butler, A., & Wang, S. (2021). Variability in QBO Temperature Anomalies on Annual and Decadal Time Scales. *Journal of Climate*, *34*(2), 589–605. https://doi.org/10.1175/JCLI-D-20-0287.1

Match, A., & Gerber, E. P. (2022). Tropospheric Expansion Under Global Warming Reduces Tropical Lower Stratospheric Ozone. *Geophysical Research Letters*, *49*(19), e2022GL099463. https://doi.org/10.1029/2022GL099463

McFarquhar, G. M., Heymsfield, A. J., Spinhirne, J., & Hart, B. (2000). Thin and Subvisual Tropopause Tropical Cirrus: Observations and Radiative Impacts. *Journal of the Atmospheric Sciences*, *57*(12), 1841–1853. https://doi.org/10.1175/1520-0469(2000)057<1841:TASTTC>2.0.CO;2

Mote, P. W., Rosenlof, K. H., McIntyre, M. E., Carr, E. S., Gille, J. C., Holton, J. R., et al. (1996). An atmospheric tape recorder: The imprint of tropical tropopause temperatures on stratospheric water vapor. *Journal of Geophysical Research: Atmospheres*, *101*(D2), 3989–4006. https://doi.org/10.1029/95JD03422

Oman, L., Waugh, D. W., Pawson, S., Stolarski, R. S., & Nielsen, J. E. (2008). Understanding the Changes of Stratospheric Water Vapor in Coupled Chemistry–Climate Model Simulations. *Journal of the Atmospheric Sciences*, *65*(10), 3278–3291. https://doi.org/10.1175/2008JAS2696.1

Ortland, D. A., & Alexander, M. J. (2014). The Residual-Mean Circulation in the Tropical Tropopause Layer Driven by Tropical Waves. *Journal of the Atmospheric Sciences*, *71*(4), 1305–1322. https://doi.org/10.1175/JAS-D-13-0100.1

Pahlavan, H. A., Fu, Q., Wallace, J. M., & Kiladis, G. N. (2021). Revisiting the Quasi-Biennial Oscillation as Seen in ERA5. Part I: Description and Momentum Budget. *Journal of the Atmospheric Sciences*, *78*(3), 673–691. https://doi.org/10.1175/JAS-D-20-0248.1

Philander, G. (1990). Geophysical Interplays: *El Niño, La Niña, and the Southern Oscillation* . S. George Philander. Academic Press, San Diego, CA, 1989. x, 293 pp., illus. $59.50. International Geophysics Series, vol. 46. *Science*, *248*(4957), 904–905. https://doi.org/10.1126/science.248.4957.904

Plumb, R. A., & Bell, R. C. (1982). Equatorial waves in steady zonal shear flow. *Quarterly Journal of the Royal Meteorological Society*, *108*(456), 313–334. https://doi.org/10.1002/qj.49710845603

Plumb, R. A., & Eluszkiewicz, J. (1999). The Brewer–Dobson Circulation: Dynamics of the Tropical Upwelling. *Journal of the Atmospheric Sciences*, *56*(6), 868–890. https://doi.org/10.1175/1520-0469(1999)056<0868:TBDCDO>2.0.CO;2

Podglajen, A., Hertzog, A., Plougonven, R., & Legras, B. (2016). Lagrangian temperature and vertical velocity fluctuations due to gravity waves in the lower stratosphere. *Geophysical Research Letters*, *43*(7), 3543–3553. https://doi.org/10.1002/2016GL068148

Podglajen, A., Plougonven, R., Hertzog, A., & Jensen, E. (2018). Impact of gravity waves on the motion and distribution of atmospheric ice particles. *Atmospheric Chemistry and Physics*, *18*(14), 10799–10823. https://doi.org/10.5194/acp-18-10799-2018

Randel, W., & Park, M. (2019). Diagnosing Observed Stratospheric Water Vapor Relationships to the Cold Point Tropical Tropopause. *Journal of Geophysical Research: Atmospheres*, *124*(13), 7018–7033. https://doi.org/10.1029/2019JD030648

Randel, W. J., & Jensen, E. J. (2013). Physical processes in the tropical tropopause layer and their roles in a changing climate. *Nature Geoscience*, *6*(3), 169–176. https://doi.org/10.1038/ngeo1733

Randel, W. J., & Wu, F. (2015). Variability of Zonal Mean Tropical Temperatures Derived from a Decade of GPS Radio Occultation Data. *Journal of the Atmospheric Sciences*, *72*(3), 1261–1275. https://doi.org/10.1175/JAS-D-14-0216.1

Randel, W. J., Wu, F., & Gaffen, D. J. (2000). Interannual variability of the tropical tropopause derived from radiosonde data and NCEP reanalyses. *Journal of Geophysical Research: Atmospheres*, *105*(D12), 15509–15523. https://doi.org/10.1029/2000JD900155

Randel, W. J., Garcia, R. R., & Wu, F. (2002). Time-Dependent Upwelling in the Tropical Lower Stratosphere Estimated from the Zonal-Mean Momentum Budget. *Journal of the Atmospheric Sciences*, *59*(13), 2141–2152. https://doi.org/10.1175/1520-0469(2002)059<2141:TDUITT>2.0.CO;2

Randel, W. J., Park, M., Wu, F., & Livesey, N. (2007). A Large Annual Cycle in Ozone above the Tropical Tropopause Linked to the Brewer–Dobson Circulation. *Journal of the Atmospheric Sciences*, *64*(12), 4479–4488. https://doi.org/10.1175/2007JAS2409.1

Randel, W. J., Garcia, R., & Wu, F. (2008). Dynamical Balances and Tropical Stratospheric Upwelling. *Journal of the Atmospheric Sciences*, *65*(11), 3584–3595. https://doi.org/10.1175/2008JAS2756.1

Randel, W. J., Garcia, R. R., Calvo, N., & Marsh, D. (2009). ENSO influence on zonal mean temperature and ozone in the tropical lower stratosphere. *Geophysical Research Letters*, *36*(15). https://doi.org/10.1029/2009GL039343

Randel, W. J., Park, M., Emmons, L., Kinnison, D., Bernath, P., Walker, K. A., et al. (2010). Asian Monsoon Transport of Pollution to the Stratosphere. *Science*, *328*(5978), 611–613. https://doi.org/10.1126/science.1182274

Read, W. G., Lambert, A., Bacmeister, J., Cofield, R. E., Christensen, L. E., Cuddy, D. T., et al. (2007). Aura Microwave Limb Sounder upper tropospheric and lower stratospheric H2O and relative humidity with respect to ice validation. *Journal of Geophysical Research (Atmospheres)*, *112*, D24S35. https://doi.org/10.1029/2007JD008752

Richter, J. H., Anstey, J. A., Butchart, N., Kawatani, Y., Meehl, G. A., Osprey, S., & Simpson, I. R. (2020). Progress in Simulating the Quasi-Biennial Oscillation in CMIP Models. *Journal of Geophysical Research: Atmospheres*, *125*(8), e2019JD032362. https://doi.org/10.1029/2019JD032362

Rosenlof, K. H. (1995). Seasonal cycle of the residual mean meridional circulation in the stratosphere. *Journal of Geophysical Research*, *100*, 5173–5191. https://doi.org/10.1029/94JD03122

Santee, M. L., Manney, G. L., Livesey, N. J., Schwartz, M. J., Neu, J. L., & Read, W. G. (2017). A comprehensive overview of the climatological composition of the Asian summer monsoon anticyclone based on 10 years of Aura Microwave Limb Sounder measurements.

Journal of Geophysical Research: Atmospheres, *122*(10), 5491–5514. https://doi.org/10.1002/2016JD026408

Santer, B. D., Sausen, R., Wigley, T. M. L., Boyle, J. S., AchutaRao, K., Doutriaux, C., et al. (2003). Behavior of tropopause height and atmospheric temperature in models, reanalyses, and observations: Decadal changes. *Journal of Geophysical Research: Atmospheres*, *108*(D1), ACL 1-1-ACL 1-22. https://doi.org/10.1029/2002JD002258

Scherllin-Pirscher, B., Deser, C., Ho, S.-P., Chou, C., Randel, W., & Kuo, Y.-H. (2012). The vertical and spatial structure of ENSO in the upper troposphere and lower stratosphere from GPS radio occultation measurements. *Geophysical Research Letters*, *39*(20). https://doi.org/10.1029/2012GL053071

Schreiner, W. s., Weiss, J. p., Anthes, R. a., Braun, J., Chu, V., Fong, J., et al. (2020). COSMIC-2 Radio Occultation Constellation: First Results. *Geophysical Research Letters*, *47*(4), e2019GL086841. https://doi.org/10.1029/2019GL086841

Shepherd, T. G., & McLandress, C. (2011). A Robust Mechanism for Strengthening of the Brewer–Dobson Circulation in Response to Climate Change: Critical-Layer Control of Subtropical Wave Breaking. *Journal of the Atmospheric Sciences*, *68*(4), 784–797. https://doi.org/10.1175/2010JAS3608.1

Sokol, A. B., & Hartmann, D. L. (2020). Tropical Anvil Clouds: Radiative Driving Toward a Preferred State. *Journal of Geophysical Research: Atmospheres*, *125*(21), e2020JD033107. https://doi.org/10.1029/2020JD033107

Solomon, S., Rosenlof, K. H., Portmann, R. W., Daniel, J. S., Davis, S. M., Sanford, T. J., & Plattner, G.-K. (2010). Contributions of Stratospheric Water Vapor to Decadal Changes in the Rate of Global Warming. *Science*, *327*(5970), 1219–1223. https://doi.org/10.1126/science.1182488

Solomon, S., Ivy, D. J., Kinnison, D., Mills, M. J., Neely, R. R., & Schmidt, A. (2016). Emergence of healing in the Antarctic ozone layer. *Science*, *353*(6296), 269–274. https://doi.org/10.1126/science.aae0061

Sunilkumar, S. V., Parameswaran, K., Rajeev, K., Krishna Murthy, B. V., Meenu, S., Mehta, S. K., & Babu, A. (2010). Semitransparent cirrus clouds in the tropical tropopause layer during two contrasting seasons. *Journal of Atmospheric and Solar-Terrestrial Physics*, *72*(9), 745–762. https://doi.org/10.1016/j.jastp.2010.03.020

Sweeney, A., Fu, Q., Interannual Variability of Zonal Mean Temperature, Water Vapor, and Clouds in the Tropical Tropopause Layer [Data set]. Zenodo. https://zenodo.org/records/10045808

Sweeney A., (2023). October 18, 2023 Release Version (1.0.0) AodhanSweeney/TTLVariability [Software]. GitHub. https://github.com/AodhanSweeney/TTLVariability

Sweeney, A., Fu, Q., Pahlavan, H. A., & Haynes, P. (2023). Seasonality of the QBO Impact on Equatorial Clouds. *Journal of Geophysical Research: Atmospheres*, *128*(7), e2022JD037737. https://doi.org/10.1029/2022JD037737

Sweeney, A. J., & Fu, Q. (2021). Diurnal Cycles of Synthetic Microwave Sounding Lower-Stratospheric Temperatures from Radio Occultation Observations, Reanalysis, and Model Simulations. *Journal of Atmospheric and Oceanic Technology*, *38*(12), 2045–2059. https://doi.org/10.1175/JTECH-D-21-0071.1

Tegtmeier, S., Anstey, J., Davis, S., Ivanciu, I., Jia, Y., McPhee, D., & Pilch Kedzierski, R. (2020). Zonal Asymmetry of the QBO Temperature Signal in the Tropical Tropopause

Region. *Geophysical Research Letters*, *47*(24), e2020GL089533. https://doi.org/10.1029/2020GL089533

Thornberry, T. D., Rollins, A. W., Avery, M. A., Woods, S., Lawson, R. P., Bui, T. V., & Gao, R.-S. (2017). Ice water content-extinction relationships and effective diameter for TTL cirrus derived from in situ measurements during ATTREX 2014. *Journal of Geophysical Research: Atmospheres*, *122*(8), 4494–4507. https://doi.org/10.1002/2016JD025948

Thorsen, T. J., Fu, Q., Comstock, J. M., Sivaraman, C., Vaughan, M. A., Winker, D. M., & Turner, D. D. (2013). Macrophysical properties of tropical cirrus clouds from the CALIPSO satellite and from ground-based micropulse and Raman lidars. *Journal of Geophysical Research: Atmospheres*, *118*(16), 9209–9220. https://doi.org/10.1002/jgrd.50691

Tian, E. W., Su, H., Tian, B., & Jiang, J. H. (2019). Interannual variations of water vapor in the tropical upper troposphere and the lower and middle stratosphere and their connections to ENSO and QBO. *Atmospheric Chemistry and Physics*, *19*(15), 9913–9926. https://doi.org/10.5194/acp-19-9913-2019

Tseng, H. -H., & Fu, Q. (2017). Tropical tropopause layer cirrus and its relation to tropopause. *Journal of Quantitative Spectroscopy and Radiative Transfer*, *188*, 118–131. https://doi.org/10.1016/j.jqsrt.2016.05.029

Tseng, Hsiu-Hui, & Fu, Q. (2017). Temperature Control of the Variability of Tropical Tropopause Layer Cirrus Clouds. *Journal of Geophysical Research: Atmospheres*, *122*(20), 11,062-11,075. https://doi.org/10.1002/2017JD027093

Tweedy, O. V., Waugh, D. W., Randel, W. J., Abalos, M., Oman, L. D., & Kinnison, D. E. (2018). The Impact of Boreal Summer ENSO Events on Tropical Lower Stratospheric

Ozone. *Journal of Geophysical Research: Atmospheres*, *123*(17), 9843–9857. https://doi.org/10.1029/2018JD029020

Ueyama, R., Jensen, E. J., Pfister, L., & Kim, J.-E. (2015). Dynamical, convective, and microphysical control on wintertime distributions of water vapor and clouds in the tropical tropopause layer. *Journal of Geophysical Research: Atmospheres*, *120*(19), 10,483-10,500. https://doi.org/10.1002/2015JD023318

Ueyama, R., Jensen, E. J., & Pfister, L. (2018). Convective Influence on the Humidity and Clouds in the Tropical Tropopause Layer During Boreal Summer. *Journal of Geophysical Research: Atmospheres*, *123*(14), 7576–7593. https://doi.org/10.1029/2018JD028674

Ventrice, M., Wheeler, M., Hendon, H., Iii, S., Thorncroft, C., & Kiladis, G. (2013). A Modified Multivariate Madden-Julian Oscillation Index Using Velocity Potential. *Monthly Weather Review*, *141*, 4197–4210. https://doi.org/10.1175/MWR-D-12-00327.1

Virts, K. S., & Wallace, J. M. (2014). Observations of Temperature, Wind, Cirrus, and Trace Gases in the Tropical Tropopause Transition Layer during the MJO. *Journal of the Atmospheric Sciences*, *71*(3), 1143–1157. https://doi.org/10.1175/JAS-D-13-0178.1

Virts, K. S., Wallace, J. M., Fu, Q., & Ackerman, T. P. (2010). Tropical Tropopause Transition Layer Cirrus as Represented by CALIPSO Lidar Observations. *Journal of the Atmospheric Sciences*, *67*(10), 3113–3129. https://doi.org/10.1175/2010JAS3412.1

Walker, J. M., Bordoni, S., & Schneider, T. (2015). Interannual Variability in the Large-Scale Dynamics of the South Asian Summer Monsoon. *Journal of Climate*, *28*(9), 3731–3750. https://doi.org/10.1175/JCLI-D-14-00612.1

Wang, M., & Fu, Q. (2021). Stratosphere-Troposphere Exchange of Air Masses and Ozone Concentrations Based on Reanalyses and Observations. *Journal of Geophysical Research: Atmospheres*, *126*(18), e2021JD035159. https://doi.org/10.1029/2021JD035159

Wang, M., & Fu, Q. (2023). Changes in Stratosphere-Troposphere Exchange of Air Mass and Ozone Concentration in CCMI Models From 1960 to 2099. *Journal of Geophysical Research: Atmospheres*, *128*(13), e2023JD038487. https://doi.org/10.1029/2023JD038487

Wang, T., Wu, D. L., Gong, J., & Tsai, V. (2019). Tropopause Laminar Cirrus and Its Role in the Lower Stratosphere Total Water Budget. *Journal of Geophysical Research: Atmospheres*, *124*(13), 7034–7052. https://doi.org/10.1029/2018JD029845

Winker, D. M., Pelon, J., Coakley, J. A., Ackerman, S. A., Charlson, R. J., Colarco, P. R., et al. (2010). The CALIPSO Mission: A Global 3D View of Aerosols and Clouds. *Bulletin of the American Meteorological Society*, *91*(9), 1211–1230. https://doi.org/10.1175/2010BAMS3009.1

Wu, Y., & Zheng, C. (2022). Summertime Transport Pathways and Dynamics From Northern India and Tibetan Plateau to the Lower Stratosphere: Insights From Idealized Tracer Experiments. *Journal of Geophysical Research: Atmospheres*, *127*(9), e2021JD036399. https://doi.org/10.1029/2021JD036399

Xie, F., Li, J., Tian, W., Li, Y., & Feng, J. (2014). Indo-Pacific Warm Pool Area Expansion, Modoki Activity and Tropical Cold-Point Tropopause Temperature Variations. *Scientific Reports*, *4*(1), 4552. https://doi.org/10.1038/srep04552

Yang, Q., Fu, Q., & Hu, Y. (2010). Radiative impacts of clouds in the tropical tropopause layer. *Journal of Geophysical Research: Atmospheres*, *115*(D4). https://doi.org/10.1029/2009JD012393

Ye, H., Dessler, A. E., & Yu, W. (2018). Effects of convective ice evaporation on interannual variability of tropical tropopause layer water vapor. *Atmospheric Chemistry and Physics*, *18*(7), 4425–4437. https://doi.org/10.5194/acp-18-4425-2018

Yoo, C., & Son, S.-W. (2016). Modulation of the boreal wintertime Madden-Julian oscillation by the stratospheric quasi-biennial oscillation. *Geophysical Research Letters*, *43*(3), 1392–1398. https://doi.org/10.1002/2016GL067762

Yulaeva, E., Holton, J. R., & Wallace, J. M. (1994). On the Cause of the Annual Cycle in Tropical Lower-Stratospheric Temperatures. *Journal of the Atmospheric Sciences*, *51*(2), 169–174. https://doi.org/10.1175/1520-0469(1994)051<0169:OTCOTA>2.0.CO;2

Zeng, Z., Sokolovskiy, S., Schreiner, W. S., & Hunt, D. (2019). Representation of Vertical Atmospheric Structures by Radio Occultation Observations in the Upper Troposphere and Lower Stratosphere: Comparison to High-Resolution Radiosonde Profiles. *Journal of Atmospheric and Oceanic Technology*, *36*(4), 655–670. https://doi.org/10.1175/JTECH-D-18-0105.1

Zhou, C., Dessler, A. E., Zelinka, M. D., Yang, P., & Wang, T. (2014). Cirrus feedback on interannual climate fluctuations. *Geophysical Research Letters*, *41*(24), 9166–9173. https://doi.org/10.1002/2014GL062095

Ziskin Ziv, S., Garfinkel, C. I., Davis, S., & Banerjee, A. (2022). The roles of the Quasi-Biennial Oscillation and El Niño for entry stratospheric water vapor in observations and coupled chemistry–ocean CCMI and CMIP6 models. *Atmospheric Chemistry and Physics*, *22*(11), 7523–7538. https://doi.org/10.5194/acp-22-7523-2022